Diogo Manuel Simões Lopes

Licenciado em Engenharia de Micro e Nanotecnologias

Low-cost upconversion nanomaterials for anti-counterfeiting solutions

Dissertação para obtenção do Grau de mestre em

Engenharia de Micro e Nanotecnologias

Orientador: Daniela da Silva Nunes Gomes, Professora Auxiliar Convidada, Faculdade de Ciências e Tecnologias, Universidade Nova de Lisboa

Co-orientador: Andreia Jóia Araújo Cardoso, Manager de Inovação, INCM

Júri:

Presidente: Prof. Dr. Rodrigo Ferrão de Paiva Martins, FCT – UNL

Arguentes: Dr. Diana Pereira Gaspar, FCT-UNL

Vogais: Prof. Dr. Daniela da Silva Nunes Gomes, FCT – UNL

FACULDADE DE CIÊNCIAS E TECNOLOGIA
UNIVERSIDADE NOVA DE LISBOA

Low-cost upconversion nanomaterials for anti-counterfeiting solutions

Acknowledgements

First of all, I would like to thank the FCT/UNL teachers for all the knowledge that has been given to me during this course and, secondly, to both institutions CENIMAT and INCM for the opportunity to carry out this final work.

Secondly, I would like to thank Professor Rodrigo Martins and Professor Elvira Fortunato for the access to these installations and technology. Their multidisciplinary knowledge, competence and commitment allow the excellent conditions of work here in CENIMAT. In addition, I would like to thank for the fact of being able to open this unique and outstanding integrated masters in Portugal.

I would like to express my gratitude to my supervisor, Professor Daniela Gomes for accepting and give me the chance to join and work in her research group. Without your help and patience this work would not be possible.

One big thank to Mariana Matias and especially to Tomás Freire, for spending several hours with me and helping since the very first moment in every way possible.

To Alexandra Gonçalves for teaching me the safety rules in a laboratory and for all the support.

There are some special thanks left for my friends that always worried about my work and were interested on its progress along the way – Manuel Oliveira and Pedro Abreu. To my car travel company Raquel Martins, who heard my complains and brought me up in my lower moments. Adriana Mateus I will forever be grateful for all the times that you made me work harder and made me a more responsible person.

A final thank to my family for all the support and belief in me, as well as for helping me to become the person I am today.

Abstract

This work consisted on the production and characterization of low-cost upconversion (UC) nanoparticles based on zirconia oxides (ZrO_2). The production was made by a hydrothermal process assisted by microwave irradiation, were 4 reagents were tested: sodium hydroxide, hexamethylenetetramine, urea and ethylenediamine. Ytterbium (Yb) and erbium (Er) were used as dopants to allow the upconversion process. The aim was that the nanoparticles would match photoluminescent characteristics of a detector provided by INCM (Imprensa Nacional – Casa da Moeda) so that it can be used as a security marker.

Hexamethylenetetramine has proven to be the best reagent to reach the desired nanoparticles with a maximum size of 100 nm. It was concluded that no dispersant was necessary to stabilize the powder when added directly into the proper ink. Different synthesis parameters were tested to optimize the morphology and size of nanomaterials such as time, pH and temperature. It was also achieved the scale up production of this nanoparticles, since passing from 25 ml to 600 ml solutions did not alter the optical response. Both flexographic and screen printing were proven successful printing methods as the final luminescent outcome matched the marker characteristics. A cheaper, environmentally friendly and new marker was accomplished, allowing that more products may have a security mark, guaranteeing their final authenticity.

Keywords: upconversion; ZrO_2; ytterbium; erbium; microwave; security marker.

Resumo

Este trabalho consistiu na produção e caracterização de partículas de baixo custo e conversão ascendente baseadas em óxidos de zircónia (ZrO_2). A produção foi feita por um processo hidrotermal assistido por microondas, onde 4 reagentes foram testados: hidróxido de sódio, hexametilenotetramina, ureia e etilenodiamina. Itérbio e érbio foram usados como dopantes para permitir o processo de conversão ascendente. O objetivo era que as nanopartículas tivessem as mesmas características de fotoluminescência que o detetor fornecido pela INCM (Imprensa Nacional – Casa da Moeda) para poder ser usado como marcador de segurança.

Hexametilenotetramina provou ser o melhor reagente para atingir as nanopartículas com tamanho máximo de 100 nm. Foi concluído não ser necessário nenhum dispersante para estabilizar o pó quando adicionado diretamente na tinta. Diferentes parâmetros de síntese foram testados para otimizar a morfologia e tamanho das nanopartículas como tempo, pH e temperatura. Foi também conseguido o processo de expansão de produção de nanopartículas, uma vez que passar de soluções de 25 ml para 600 ml não alterou a resposta ótica. Tanto a flexografia como o *screen printing* demonstraram ser métodos capazes, pois o resultado final de luminescência correspondeu com as características do marcador. Um marcador novo, mais barato e amigo do ambiente foi conseguido, permitindo que mais produtos possam tem uma marca de segurança, garantindo a sua autenticidade final.

Palavras-chave: conversão ascendente; ZrO_2; itérbio; érbio; microondas; marcador de segurança.

Table of contents

List of Figures

List of tables

Symbols

min – Minutes

h – Hour

mM – Millimolar

°C – Degree Celsius

rpm – Rotations per minute

cmHg – Centimetres of Mercury

Acronyms

UC – Upconversion

INCM – Imprensa Nacional - Casa da Moeda

RE – Rare Earth

IUPAC – International Union of Pure and Applied Chemistry

XRD – X-ray diffraction

SEM – Scanning electron microscopy

EDS – Energy-dispersive X-ray spectroscopy

UV – Ultraviolet

IR – Infrared radiation

NIR – Near-infrared

PL – Photoluminescence

Objectives

Among the several security measures existent, security ink is one used by INCM. It is not produced by the INCM, but outsourced by other companies instead. There are different materials that can be used for this intent and if it is possible to use cheaper materials they will be used. This was the main objective of this work:

- Production of a replica nano-marker by the one that already exists, using ZrO_2 as a matrix doped with Yb3+;
- Scale-up process from 25 ml to 600 ml maintaining particle size and luminescent properties;
- Production of a developed nano-marker with the same base material and synthesis parameters, by adding 1 more dopant;
- Well dispersion of the produced nano-markers into the INCM ink and its posterior printing.

Motivation

Counterfeiting is sufficiently prevalent throughout history that it has been called "the world's second oldest profession" [1]. Counterfeit currency has been in circulation for nearly as long as currency itself. Long before bills were used as form of money, counterfeiters would alter others forms of currency to gain more value than the traded item was worth. One of the first instances of this was during the foundation of the American colonies, when Native Americans would trade shells as a form of currency [2]. Blue-black shells, which were rarer, had more value than their white counterparts. As a result, some traders would die the white shells a blue-black colour and pass them off at higher value. From shells it passed to the coins, followed by bills and then, at some point, to everything that can be bought.

From the perspective of the person that holds the fake object, counterfeiting can be seen as deceptive or nondeceptive [3]. Deceptive counterfeiting involves purchases in which consumers are not aware that the product they are buying is a counterfeit, as is often the case in categories such as automotive parts, consumer electronics, and pharmaceuticals. In other categories, however, consumers are typically aware that they are purchasing counterfeits. This is known as nondeceptive counterfeiting [4].

Entities and regulations have been created to fight back this never-ending problem. In Portugal the most important organization, responsible for these actions, is INCM. There are several methods used to guarantee the authenticity of different products, some more efficient than other. Having a method rapidly and easy to apply allows that a vast majority of brands are capable of having a safety measure. Security inks are a great deal in this field. The desire in this thesis was to formulate a low-cost security ink as a way of fighting back the counterfeit market.

1 Introduction

Counterfeit means to imitate something authentic, with the intent to steal, destroy, or replace the original, for use in illegal transactions. The counterfeit market continues to increase over the years, not only in goods such as clothing, pharmaceuticals, and electronics, but documents and currency as well. This problem harms two publics: legitimate producers and society. For legitimate producers, the primary problem is losing sales and associated revenues. In terms of society, it was found significant effects on the job market through the displacement of legitimate economic activity by counterfeiting and piracy [5].

Furthermore, it was estimated net job losses in 2013 to lie, globally, between $2 and $2.6 million, and projected net job losses of $4.2 to $5.4 million by 2022 [6]. To fight back this problem the race in technological advances has expanded, being necessary the evolution of new detection ways in order to get around the problem.

Between the methods already used, such as radio frequency identification tags, nuclear track technology, or laser holograms, another alternative to overcome this problem is to introduce security inks [7–12]. These inks are a specialised segment of printing inks, fulfilling the role of security in addition to their colouring function. Integrated as a security feature on documents, these inks can be tactile, coloured with or without colour shifting attributes and other optical effects. Taggants are uniquely encoded materials that are virtually impossible to duplicate. These can be added to the particles contained in the ink, that work as fingerprint, being one of the most important aspects in this work [14]. These taggants are the materials that turn normal inks into security inks. Some of security inks are luminescent inks and their exclusive optical properties allow the possibility of creating complicated patterns. Besides this advantageous property, it is remarkable that the normal detectors used for these analyses are cheap and readily available [10]. The use of these inks has been around for some decades, however, new advances in technology brought some novelty in this area – upconverting nanoparticles inks [11]. UC nanoparticles are spectroscopy taggants. This new evolution makes them more difficult to replicate and increases safety both for customers and manufacturers [12,15].

There is a considerable amount of potential improvements in using upconversion inks when compared to downconversion inks, in which the latter shows fluorescence effect when they are UV radiated. In the first place, the ink produced with upconversion materials, and its own reading device, are more difficult to replicate than inks that are UV radiated. Not only are they harder to replicate, but it is also possible to prepare these inks that only show the colour wanted, under specific excitation power intensities, creating one more barrier for falsification. Finally, it is possible to print the patterns desired on top of highly fluorescent surfaces since near infrared excitations will not excite downconversion materials [11].

The main objective of this thesis is to produce low-cost upconversion nanoparticles by microwave synthesis that will be further integrated in inks with posterior printing, guaranteeing the final product authenticity. These nanoparticles are based on metal oxides (matrix) containing rare earth (RE) dopants Ytterbium (Yb) and Erbium (Er). The chosen matrix will be Zirconia oxide (ZrO_2), which is an abundant material, inexpensive and easily synthesized by chemical synthesis routes [16]. Yttria based materials have been extensively studied and analysed for

upconversion luminescent purposes [11,12,17–21], but since Zirconia is cheaper, more abundant in the earth's crust and has similar characteristics [22–24] makes it a perfect replace candidate.

1.1 Upconversion

1.1.1 Upconversion process

Upconversion, which was first proposed by Nicolaas Bloembergen in the mid-1960, has received considerable attention throughout the last decades due to its possible applications in modern technology [25,26]. This phenomenon can be seen as the process where two or more low energy photons excite an ion into a higher energy state and a single, high energetic, photon is emitted when the ion transits to the ground state [27].

Stokes shift is a difference, in wavenumber or frequency units, between positions of the band maxima of the absorption and emission spectra of the same electronic transition, being two examples fluorescence and Raman. It was named after Irish physicist George Gabriel Stokes [28,29]. When a system, being a molecule or atom, absorbs a photon it gains energy and enters an excited state. One way for the system to relax is to reemit a photon, which is losing its energy. Another method would be the loss of energy as heat – when the emitted photon has less energy than the absorbed photon this energy difference is called Stokes shift.

On the other hand, in the case of anti-stokes shift, the absorbed energy by the photon is lower than the emitted energy, which is violating Stokes law in its basic statement [30]. Not only is the photon absorbed by a molecule, but collision with other particles from the mesh gives energy to the particle. Therefore, this particle receives more energy than the one given from the absorbed photon, making the particle to go into a superexcited state [31,32]. Consequently, upconversion mechanism is an anti-stokes emission. Generally, near-infrared photons are used to excite these particles which will emit visible light, that has a smaller wavelength and is more energetic. There are two major qualities about using near infrared excitation: great sample penetration compared to ultraviolet excitation and is less harmful to biological samples [33].

The upconversion process is made up of two kinds of molecules – a sensitizer and an emitter. These molecules have three different important states. The first one is the ground state, the lowest energy state. Then, there are two kinds of excited states that can be presented after energy has been added from light being absorbed. Triplet state can store energy and the singlet state that takes energy and releases it as light [34,35].

An energy schematic of the photon upconversion process is shown in Figure 1.1. The first step of this process starts with the transition from ground state (S_0) to a singlet state (S_1) of one sensitizer by energy absorption(1a). The singlet state in the sensitizer is then converted into a triplet state to store energy (2a). This transition occurs to prevent singlet state to emit light. Next, the triplet state needs to be transferred from the sensitizer molecule to an emitter molecule (3a). Electrons are exchanged between the sensitizer molecule and the emitter molecule, which allows the energy from the triplet state to move. These processes need to happen many times in parallel so that once many emitter molecules have got triplet excited states in them annihilation phenomenon can begin. It happens when two triplet states are close together, they destroy each other – in one molecule the triplet is changed to ground state (4a) and the other takes that energy, adds it to its own energy, and goes from a triplet excited state to a singlet excited state (4b).

Finally, a singlet excited state of the emitter molecule emits light, bringing all our molecules now into the ground state, back where it started (5) [36–38].

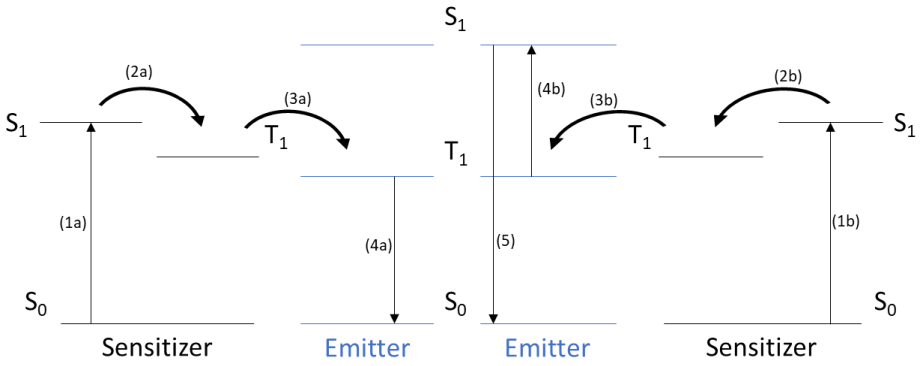

Figure 1.1 – Energy level diagram characterizing Energy Transfer Upconversion process. Adapted from [36].

Energy Transfer Upconversion (ETU) mechanism is represented above, being the most efficient method but there are two others main upconversion mechanisms – Excited State Absorption (ESA) and Photon Avalanche (PA) [39–41]. The ESA process is a successive absorption of two photons from a lower excited state to a higher excited state of an atom, molecule or ion. It can occur only after an electron has already been excited to the lower excited state [42]. The principle of PA is characterised by a pump beam which is only resonant with a transition between excited states. It requires a minimum excitation power called the threshold value so that the process initiates. Essentially, it is a loop process where simultaneously happens ESA mechanisms to excite light and cross relaxation. [40–44].

Phosphors are substances that exhibit the phenomenon of luminescence being lighting the most important application. Downconversion is a common property seen in these substances [45]. An example of this process is when ultraviolet light (radiation with shorter wavelength) is used to excite visible light wavelength photons [33]. Some properties associated with downconversion materials are not valuable, for instance, the high toxicity and easy duplication. For this reason, it is expected that upconversion materials replace the downconversion materials in some cases, such as security printing. The development in this area has allowed advances in some fields of technology such as biological labelling, bioimaging, biosensors ant temperature sensors, drug release and delivery, photo and displays [46–51].

1.1.2 Upconversion materials

According with IUPAC, rare earth materials are composed by 17 chemical elements – 15 lanthanides (lanthanum, cerium, praseodymium, neodymium, promethium, samarium, europium, gadolinium, terbium, dysprosium, holmium, erbium, thulium, ytterbium, and lutetium), scandium and yttrium. The last two, even though having different electronic and magnetic properties, are considered RE elements because of their tendency to occur in the same natural rock deposits as the lanthanides and exhibit similar chemical and physical properties [52].

Many types of equipment are in great need of RE doped ions such as wind turbines, hybrid cars, optoelectronic equipment, biological fluorescence labelling, refining crude oil and many more [53–55]. The use of this elements has resulted in major enhancements in the performance of these applications, including efficiency, longevity and reliability besides the reduction in

volume and weight of the systems that they are used [56]. Because their good properties, lanthanides have received considerable attention for doping purposes.

On the present work, Yb will have special attention, as it will be the dopant most used in the Zirconia matrix. RE 3+ dopants have unique characteristics that are required for upconversion purposes such as intraconfigurational transitions. In the case of Yb3+ only one excited state is found matching well f-f transitions – $^2F_{5/2}$. The $^2F_{5/2} \rightarrow {}^2F_{7/2}$ is the principal transition in the emission spectra utilized in upconversion [41]. Transitions between these energetic levels are forbidden, but when RE are inside specific lattices, such inorganic lattices, these rules can be overtaken. This material is one of the best choices, among all the RE ions due its absorption cross section being large at 980 nm [47,57]. Yb works well with other dopants (especially with Er [58]) and in this work it will be used both as single doping element and co-doped with Er.

The properties of the host lattice and its interaction with the dopant ions have a strong influence on the UC process. In this work, ZrO_2 will be used as host matrix and its properties will be studied. Commonly, undoped ZrO_2 presents monoclinic structure, but the introduction of RE dopant stabilizes the tetragonal crystalline phase [43]. Moreover, the ZrO_2 lattice is chemically, photothermally, and photochemically highly stable and has a broad optical transparency from the visible to the NIR, making it a good ceramic oxide for upconversion photonic applications [59–61].

W. J. Yao, *et al.* [12] has reported the synthesis of lanthanides Er, Yb and europium (Eu), by a hydrothermal method, in a large scale, to synthesize materials used in inks to apply in anti-counterfeiting printing. The method used to produce such particles has a great effect on their final performance, so the selection of production technique and parameters used are of extreme importance.

1.2 Nanoparticle synthesis

Social conscience and economic factors are great concerns for today´s consumers and society. The combination of eco-friendly and low-cost methods are especially desired qualities in the processes of synthesis [62]. There are some different ways of synthesising nanoparticles such as coprecipitation, sol-gel, hydrothermal method, microemulsion and microwave-assisted, among others [63–68].

Hydrothermal synthesis refers to heterogeneous chemical reactions of materials in aqueous media above 100 °C and 1 bar in a sealed vessel. In nature, it is possible to observe this type of reaction achieving the conditions required for mineral formation [62]. Like the name suggests, this method uses water as a solvent, which has good qualities. Not only the water is abundant in the world, but it also has some useful properties – water molecules have polarity, one end has a partially negative charge and the other end has partially positive charges which lead to hydrogen bonds. This is the critical feature that makes the water a suitable solvent for a large class of molecules. Every molecule that has charge, or that is polar, tends to dissolve well in water – they can be called hydrophilic. On the other hand, molecules that are not polar or charged, alkanes or oils, for example, will not dissolve in water and will form clusters – hydrophobic molecules.

Between different ways of heating the solution, microwave is considered a simple, fast and cheap method that offers high efficiency and reproducibility. Moreover, microwave-assisted

synthesis provides the opportunity to complete reactions in minutes with uniform heating, since microwaves can transfer energy directly to the reactive species, promoting transformations that are difficult to obtain using conventional heating. Microwaves are a type of electromagnetic energy with frequencies in the range of 300 MHz to 300 GHz. Interactions between materials and microwaves are based on two specific mechanisms: dipole interactions and ionic conduction. Both mechanisms require effective coupling between components of the target material and the rapidly oscillating electric field of the microwaves [64]. Conventional heating by conduction will induce convection currents inside the material so that the temperature can spread, being slower and energetic inefficient [69–71].

Synthesizing both pure and doped ZrO_2 nanoparticles, by microwave route, has been previously reported with interesting results [72,73]. Gnanamoorthi *et al* (2015) demonstrated that the average crystalline size of pure ZrO_2 is 40 nm and doped with Ce (cerium) with 5 to 15 % only changed the average size in 6 nm [74]. Also demonstrated that agglomerated crystallites were smaller for doped ZrO_2 that for pure ZrO_2. Opalinska *et al* concluded that different pressures on the microwave synthesis induced different grain sizes on Pr (Praseodymium) doped ZrO_2 powders from 9 to 17 nm [75].

Therefore, in this thesis, hydrothermal synthesis using microwaves was the chosen technique to produce the nanoparticles. Once this step was completed and the particles were formed, they did not present the required intrinsic properties (such as high crystallinity and fully distribution of the dopant in the matrix), adding the need to an annealing process [76]. Recrystallization, growth of the nanoparticles and fully evaporation of solvents are 3 crucial changes experienced in this annealing process, altering the final luminescence of the material [46,77].

1.2.1 Annealing treatment

Annealing, in metallurgy and materials science, is a heat treatment that alters the physical and sometimes the chemical properties of a material to either increase or reduce its ductility and its hardness, making it more workable [78]. It involves heating a material above its recrystallization temperature, maintaining a suitable temperature followed by slowly cooling.

As described by M. R. Gauna, *et al.* [79] pure Zirconia (ZrO_2) presents monoclinic phase below 1170 °C, tetragonal between 1170 and 2370 °C and above this temperature transits to cubic ZrO_2. This temperature values change when the material is doped and vary according to the amount of stabilizer or pH values during the synthesis route [80]. In order to reduce energy consumption in the overall synthesis process, the lower temperature for this stage will be used. This operation concludes the particles treatment, making them ready to be combined with the proper ink.

1.3 Ink Production

There are several printing methods available, and some are simple, low-cost and can be rapidly produced to originate uniform materials. Two methods were selected for the present work, which is screen-printing and flexographic.

A screen-printing system, as illustrated in Figure 1.2 (a), consists of a flat support with a patronized screen within frame. The printing technique involves spreading an amount of ink through the screen with the help of a squeegee, allowing the ink to pass throw the permeable areas and form the desired pattern in the substrate. Screen printing technique allows the printing of patterns of minimum 10 µm, with thickness ranging from 5 to 100 µm, depending on the mesh size and ink composition [81–84]. It is a favourable way for customization of documents.

Flexographic printing, most often called flexo [85], is a form of relief printing where ink is applied to a raised image on a flexible plate then impressed onto a substrate as shown in Figure 1.2 (b). The main reason for selecting the use of flexo printing was because it is a similar printing technique as the one most used in INCM (Imprensa Nacional – Casa da Moeda). This process has grown in recent years because of improvements in print quality, the capability to print on many substrates and the use of environmentally responsible water-based inks. Some of the more interesting facets of flexo printing is the ability to reverse print artwork, being able to achieve increased printing speeds (approximately 10 m^2/s) and resolutions of 50 to 100 µm [86,87].

This work is a collaboration with INCM which is the institution in charge of the production of goods and services fundamental to the functioning of the Portuguese State, travel documents and the minting of coins [88]. It is presented a cheaper solution that can impact the cost on security inks production. Research and development are not only about discovering something new but also inexpensive alternatives.

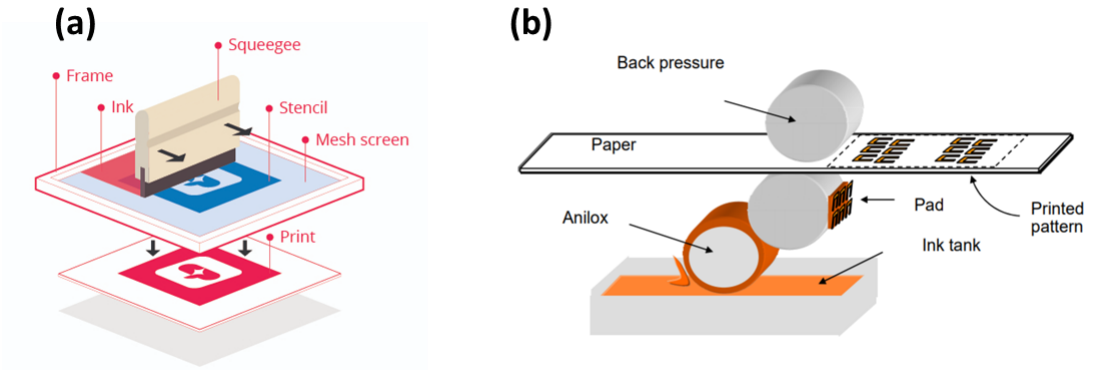

Figure 1.2 – (a) Schematic of a screen-printing stage, copied from [83], (b) Flexographic principle, copied from [86].

2 Experimental Sections

2.1 Nanoparticles Production

This dissertation was done in CENIMAT, where the main goal was to find a replica of a commercial marker used by the INCM – ZrO_2:Yb3+. A second objective was to try to make a second marker, adopting a second RE, increasing its security – ZrO_2:Yb3+/Er3+. With the purpose of enabling the security ink to work, nanoparticles with specific luminescent properties were added to an existent ink. The required properties for these nanoparticles were directly related with the detector provided by INCM, so that validation could be done accordingly. It is not the main matrix of the nanoparticles that influences the response, but the dopant used. Hence, the dopant and its percentage on the matrix were not changed from the work previously done that followed the same line of work – 1.5% Yb. However, since a new material was being used, other changes were applied.

The starting reagents were Zirconium acetate ($C_4H_6O_4Zr$) CAS: 7585-20-8 from Aldrich, Ytterbium (lll) nitrate pentahydrate ($N_3O_9Yb \cdot 5H_2O$) CAS: 35725-34-9, purity 99.9% from Sigma-Aldrich, Erbium (lll) acetate hydrate ($C_6H_9ErO_6 \cdot xH_2O$) CAS:207234-04-6, purity 99.9%, from Sigma-Aldrich, Urea (CH_4N_2O) CAS: 57-13-6 purity ≥98 % from Sigma Aldrich, Sodium hydroxide ($NaOH$) CAS: 1310-73-2, purity ≥98% from Labkem, Hexamethylenetetramine or HMT ($C_6H_{12}N_4$) CAS: 100-97-0, purity ≥99.5% from Sigma-Aldrich, Ethylenediamine or EDA ($C_2H_8N_2$) CAS: 107-15-3, purity ≥99% from Sigma-Aldrich, Triton X-100 ($C_{16}H_{26}O_2$) CAS: 09002-93-1, from J.T. Baker and Polyvinylpyrrolidone or PVP (C_6H_9NO) CAS: 9003-39-8, from Aldrich.

The reasons for choosing these 4 reagents can be summarized to: Urea was used in a similar work with a different matrix material and this time was tried out with ZrO_2. Sodium Hydroxide was used to study the pH effect on the whole process. Hexamethylenetetramine works as a good stabilizing agent and ethylenediamine being another amine was also tried for comparison purposes.

The amount of the two first reagents was fixed at 0.0025 M of zirconium and 0.0375 mM of ytterbium (1.5% in molar percentage of the zirconium), dissolved in 100 ml of water. These quantities were used in every initial solution, changing the precursor as a result of studying which would originate better outcomes, not only in terms of luminescent response, but particle size as well. Four distinct precursors were prepared using urea, sodium hydroxide, hexamethylenetetramine, and ethylenediamine. In the case of the NaOH, a dilution in water was first made to obtain a concentration of 5 M. The precursors used for the study of ZrO_2:Yb3+ varied in the quantities showed below:

- When using urea, the amounts used were 0.5, 0.75 and 1 g;
- To study the difference in pH NaOH was added until the pH was 5, 7, 9, 13;
- The concentrations of HMT were 2, 25, 50 and 100 mM;
- Lastly, 0.5 g of ethylenediamine was tested.

Adding each one of these, in separate samples, allowed to analyse what reagent was more favourable for the microwave reaction. Before each sample goes to the microwave, a 5 min

stirring was required to make the solution homogeneous using an Heidolph Hei-End Instrument and then transferred to a pyrex vessel. Samples that contained NaOH needed a security teflon protection inside the vessel.

Additionally, different reaction parameters were used for comparison reasons. The microwave CEM Discover SP microwave was used, which permitted the control of temperature, time, pressure, power and stirring. On a first stage, temperature was studied varying between 140, 160, 180 and 200 °C. On a second stage, different synthesis times were used: 15, 25, 45 and 90 min.

After microwave synthesis, the powder produced was steadily cleaned. The first step was to decant the remaining liquid from the reaction, leaving the nanoparticles on the bottom and refill with distilled water. Then, the particles were put inside an appropriate vessel to be cleaned in the Neya 16 centrifuge. This process was repeated 6 times, the first 3 with distilled water and another 3 with isopropanol (IPA – C_3H_8O) using 4000 rpm over 5 min each time, removing the excess liquid at the end of each centrifugation. Thereafter, a drying process, to remove most of the solvents was carried away using an exicator for at least 5 hours at 60 °C and -60 cmHg of pressure.

Lastly, the final step was the annealing treatment using a Naberther furnace. Zirconia doped particles were submitted to 800, 900 and 1000 °C, over 4 h plus 1 h ramping with normal air atmosphere. This phase owed to an increase of grain size, doping homogeneously and evaporation of all solvents [15,43-44] achieving ZrO_2: Yb3+.

Once the whole steps of synthesis were completed and the particles were achieved, to assure reproducibility at industrial scale, the CEM Mars One microwave (that has the capacity to synthesize 600 ml) was utilized instead of the Discover SP. The parameters that showed better outcomes were utilized: 180 °C, for 25 min.

For the second marker (developed marker) Yb and Er were both used in the same matrix with concentrations of 10 mol % and 1.625 mol %, respectively, whereas Zr concentration was not altered forming ZrO_2:Yb3+/Er3+. The reagent used was HMT, with 25 mM.

2.2 Ink Formulation and Printing

Once the particles were ready and annealed, manual mixing with the ink was the next step. The ink used was NUV 10520 Uviseal Heat Laminating Transparent White from Apollo Inks & Coating Int. Large particles were not desired for the mix since they are too heavy and would fall to the bottom, resulting in sedimentation. To make them smaller enough, and to stabilize into a homogenous suspension, the particles ZrO_2: Yb3+ (HMT) were grinded with a mortar and pestle. Figure 2.1 illustrates the result.

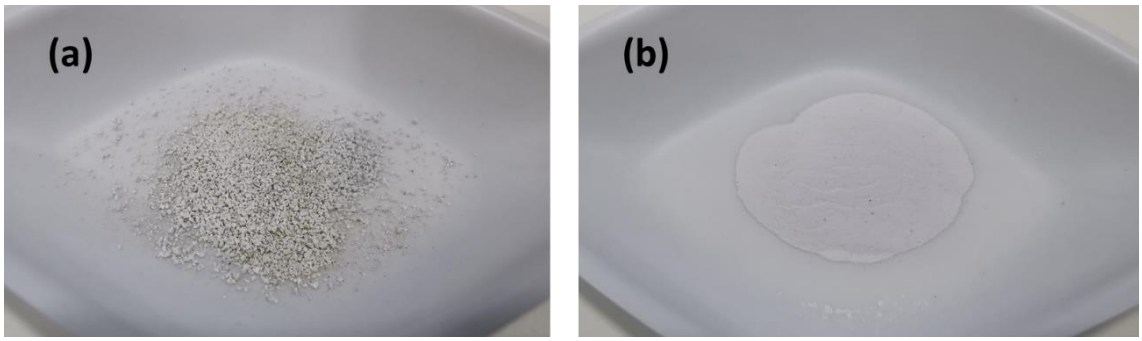

Figure 2.1 - (a) Resultant powder on the final process, (b) grinded powder.

For the purpose of dispersion of the nanoparticles the dispersants Triton X-100 (non-ionic surfactant) and PVP (water-soluble polymer) were applied. The first dispersion was carried out diluting 12 mg of Triton in 20 ml of H_2O. This solution was mixed with 0.2 g of particles and then to 0.4 g of ink. A second dispersion was made starting with the same amounts of Triton and H_2O. Heated up until 67 °C and added 0.275 g of PVP. Then, following the same 1:2 proportion, 0.2 g of powder and 0.4 of ink were added. Different proportions of particles/ink were also tested: 1:4, 1:10, 1:20, 1:50, 1:100 and 1:500.

For the flexographic printing a RK Flexiproof 100 was used with an anilox that supported 13 and 18 cm^3/m^2 of ink. The speed was set to 20 m/min and two different pairs of pressure were used – 40 for the substrate and 70 for anilox and then 80 for the substrate and 40 for anilox. For the screen-printing method a 77T screen was used. One layer was tested in both procedures twice. The substrate used for these printings was a coated paper, that was supplied by INCM. The last step to conclude the impressed inks was a 10 min UV irradiation using a Digital UV Ozone system, from Novascan, without temperature.

2.3 Characterization Techniques

Different techniques were used with the interest of characterize the various morphologic, elemental and structural parameters. The morphology of nanoparticles was examined by scanning electron microscope SEM-FIB microscope AURIGA from Carl Zeiss (5 kV). The microscope is coupled with an energy dispersive X-ray spectroscopy (EDS) detector that was used for elemental analysis. The dimensions of the nanostructures have been determined from SEM micrographs using the ImageJ [89] software and considering 20 distinct structures for each measurement.

X-ray diffraction (XRD) was used to study the phases of the materials and their crystallinity in a PANalytical's X'Pert PRO MRD with Cu Kα radiation (λ = 1.5405 Å) and scan step size of 0.0334 degrees, from 20 to 90 °.

Photoluminescence was also examined with a 976 laser (Avantes NIR light, power source 2.5W) and 2 detectors. The first was an IR detector between 800 and 1800 nm and then a visible detector between 200 and 1200 nm.

Further characterization was performed by Raman spectroscopy (LabRAM HR Evolution, 523 nm laser, 50 LWD).

3 Results and discussion

In this section the different attempts were investigated to produce the final nano-marker using zirconia oxide as the matrix and to achieve the best structural and optical characteristics. The production of the replica of the commercial marker was the primary objective of the thesis, followed by the development of a nano-marker with two dopants in its structure. In the first stage of the study Discover SP microwave was used and only after understanding the best parameters CEM Mars One microwave was used. In the last part of this thesis, the developed marker was optimized and tested. Inks containing both nano-markers have been produced and investigated.

3.1 Detector

A detector is a device whose purpose is to signal the presence of a substance or a body in a given environment. INCM provided a detector to validate the replica marker being produced. This detector was utilized since the very early stage of this work, nanoparticle synthesis, until the latest, post printing validation, allowing insurance in every step, that the required properties were in agreement.

The detector in question can exhibit three possible responses: Green light or “tag08”, which represents positive identification of the fingerprint photoluminescent effect, orange light or “other tag”, when it recognises similar synthesis marker and red light when nothing is recognized. Being “tag08” the goal, a green frame around each SEM image was drawn to represent that the nanoparticles represented by that image passed on the detector. Furthermore, it was perceived that instead of touching the glass, it is more likely to have a better detection when some space (~2 cm) is given between the sample and the red line glass.

There are 2 windows on the detector with different objectives. One window is a motion sensor that causes the device to start working and a second window with exciting LEDs and a phosphorescence sensor. These LEDs are used to excite the sample and the detector measures twice the intensity to analyse the sample’s lifetime. A schematic of the detector is demonstrated in Figure 3.1.

In addition of complying with the optic properties, so that it passes on the detector, alterations were done in order to obtain the best size, geometry and disperse particles.

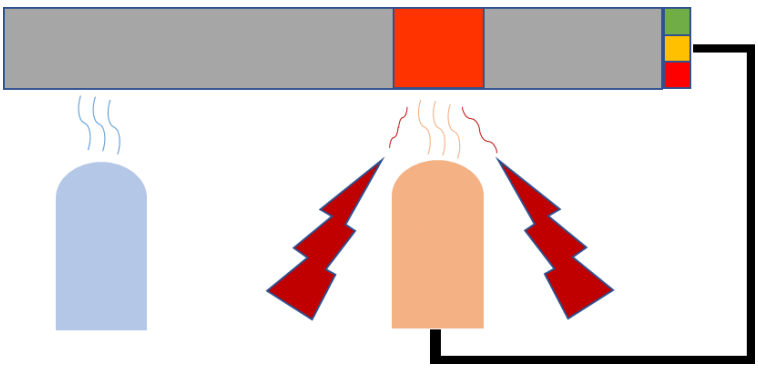

Figure 3.1 – Schematic of the detector. In blue the motion detector, in red both LEDs and orange the sensor.

3.2 ZrO_2: Yb3+ (NaOH)

3.2.1 Annealing temperature

Thermal treatment can, not only induce amorphous to crystalline phase transformation but crystalline to crystalline phase as well on ZrO_2 [90]. Several cations, such as Ca2+, Yb3+ or Er3+, can stabilize partially tetragonal phase at room temperature and monoclinic phase can also exists at room temperature [79], making it important an analysis on the phase present when using different reagents.

As said before, an annealing treatment was required to evaporate all solvents and increase crystallinity. Out of all attempts, no powder passed the detector without annealing treatment, turning this step mandatory.

The aim to find a cheaper marker not only requires using cheap materials but also an attempt to use the devices for less time and at lower temperatures to save energy. Three different temperatures were used in the thermal treatment using the same input nanoparticles. The pH in the initial solution was 5 and 200 °C was the microwave synthesis temperature for 15 min. The XRD results are shown in Figure 3.2.

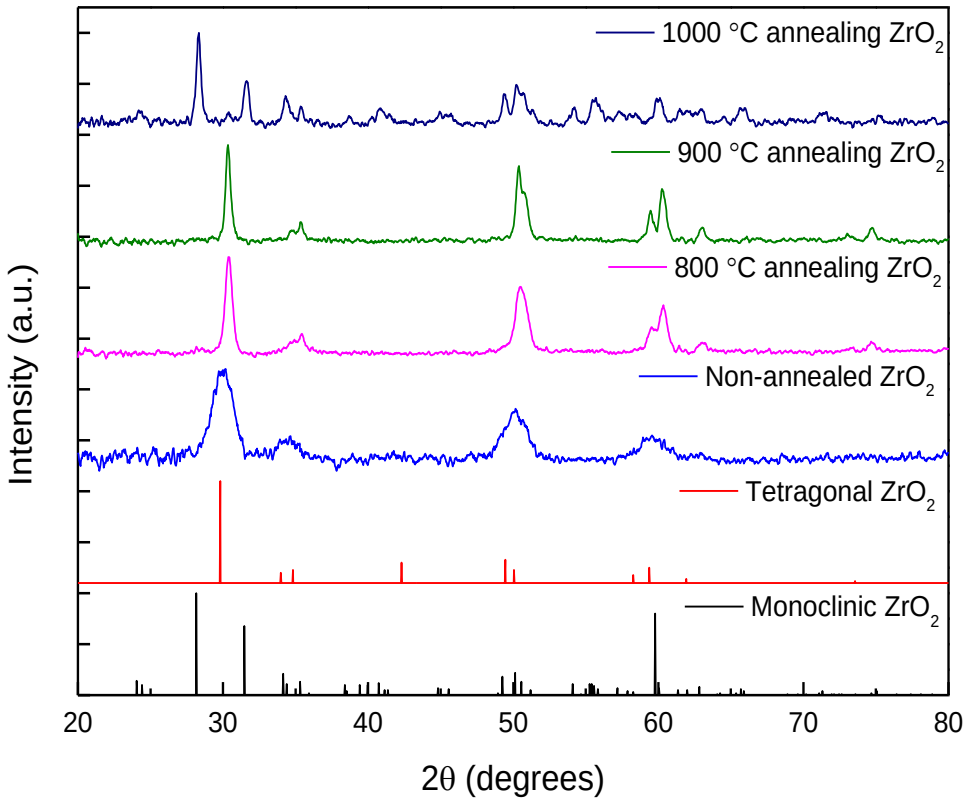

Figure 3.2 – XRD diffractograms of ZrO_2: 0.015Yb3+ (NaOH) non-annealed, annealed with 3 different temperatures and standard data from JCPDS cards 37-1484 and 24-1164. 800 °C, 900 °C, 1000 °C and simulated tetragonal and monoclinic phases.

Analysing the figure, it was possible to take some conclusions. In first place, the powder without annealing shows some crystallinity but it can be increased when annealed as the peaks get thinner and sharper. From non-annealing to annealing at 900 °C the phase present is tetragonal

as the peaks at 2θ = 30.2°, 35.2°, 50.6° and 60.2° corresponding to (101), (110), (112) and (211) planes that are characteristics of tetragonal phase of ZrO_2 [91]. The nonexistence of other peaks suggests that there are no mixture from other phases. As the annealing temperature increases to 1000 °C, a phase transformation appears: tetragonal to monoclinic. Treatments at temperatures above 1000 °C are likely to transform more Zirconia tetragonal to monoclinic.

In Figure 3.3 SEM images show the synthesized particles in the last stage, after the annealing process. Heat treatment at 800 °C resulted in nanoparticles that did not pass on the detector. It is also noticeable that both in (a) and (b) particles are agglomerated. Both 900 and 1000 °C was enough temperature for the powder to pass on the detector, but 1000 °C causes the particles to be more dispersed.

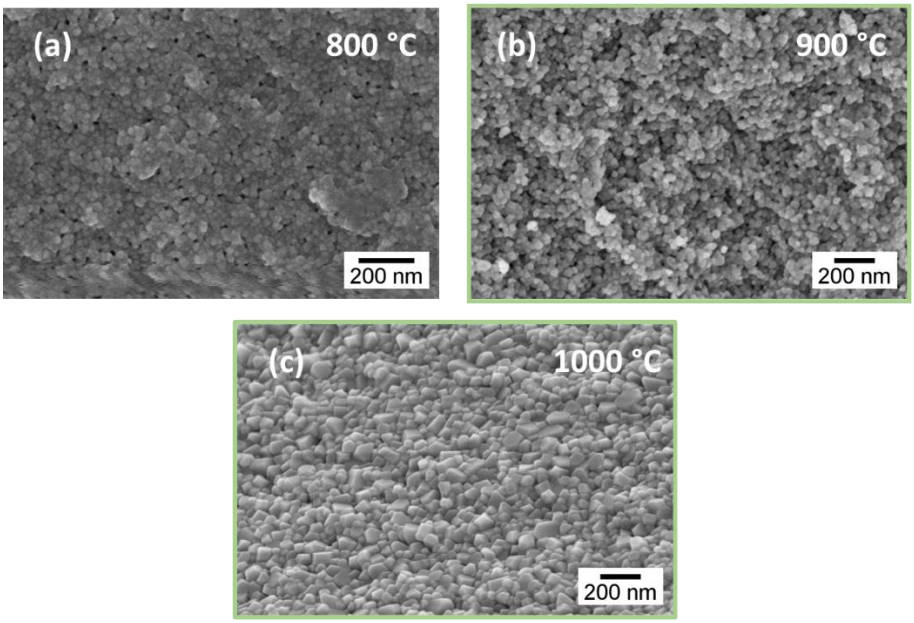

Figure 3.3 – SEM images of annealed ZrO_2: 0.015 Yb3+ (NaOH). (a) 800 °C, (b) 900 °C, (c) 1000 °C.

The particles have been measured and the results are presented in Table 3.1. In appendix can be seen a representation of measures taken from Figure 3.3 (c), were 20 random particles were used. The increase in size is considerable when comparing both temperatures as they grown more than double – 33 and 72 nm for 900 and 1000 °C, respectively. Research developed by Freire T. (2018) on a similar work, using Yttria, concluded that the best temperature was 1000 °C for this process [92]. Henceforth, the temperature for the thermal treatment was set to 1000 °C for the trials for all the reagents.

In terms of morphology, it was also noticed that the final geometry is not completely homogeneous but the shapes are similar to some extent. M. R. Gauna, when analysing pure monoclinic and 3 mol % Yttria-partially-stabilized tetragonal Zirconia, concluded that both materials presented a spherical geometry [79]. In this case, the results obtained demonstrate a geometry with flatter surfaces but overall resembling spheres, known as faceted particles [93].

Table 3.1 – Size measurements of ZrO_2: 0.015 Yb3+ (NaOH) particles annealed at 900 and 1000 °C.

ZrO2: Yb3+ (NaOH) pH 5, 900 °C	33 ± 4 nm
ZrO2: Yb3+ (NaOH) pH 5, 1000 °C	70 ± 11 nm

3.2.2 Hydrothermal synthesis pH, time and temperature

The pH on the solution has a strong effect on the structure and microstructure of the obtained ZrO_2 powders [94]. To understand the influence of pH on the hydrothermal synthesis different amounts of NaOH were used. Besides trying to figure out the best synthesis pH, an attempt of discovering the most suitable synthesis time and temperature were carried out. First, the microwave temperature was set to 200 °C changing pH (from the initial 3.5) and time. Only when these two parameters (pH and time) were determined, lower temperatures were tested, in an attempt of reducing energy used in CEM Discover SP microwave.

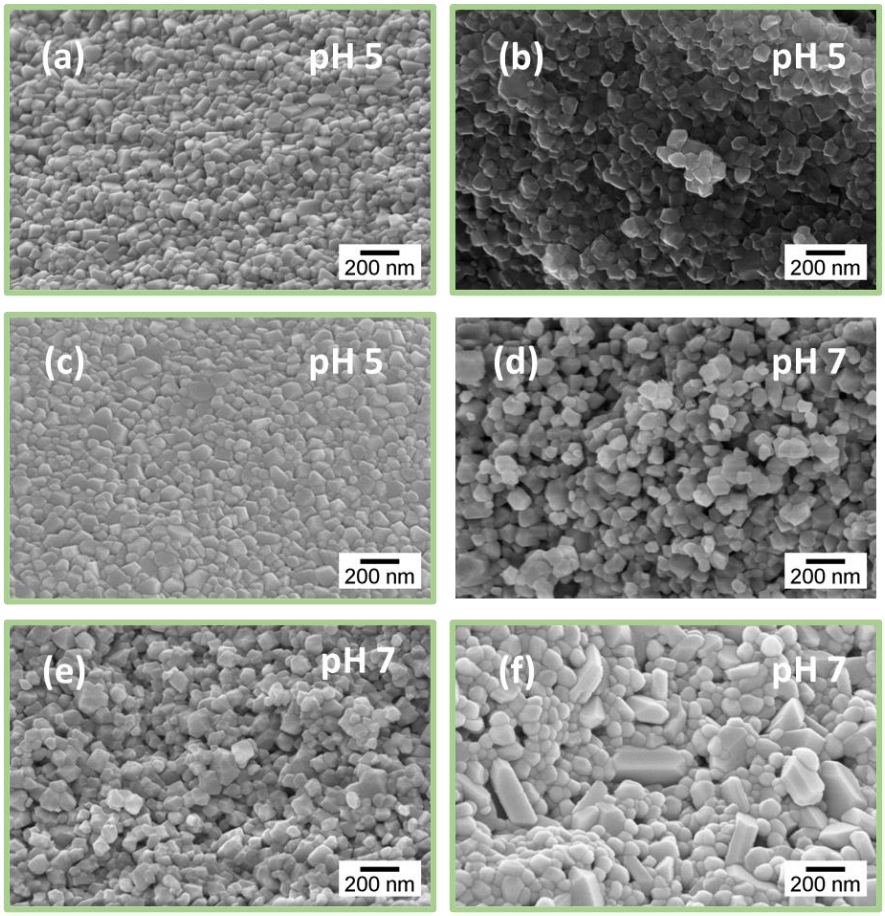

Figure 3.4 – SEM images of different pH and time synthesis of ZrO_2: 0.015 Yb3+ (NaOH). (a) 15 min, (b) 25 min, (c) 45 min with pH 5, and (d) 15 min, (d) 25 min and (f) 45 min with pH 7.

From the following analyses, most solutions with pH 5 or 7 resulted in nanoparticles that exhibited “tag08”, as it can be seen in Figure 3.4. When the pH was higher, 9 and 13, “other tag” or orange light appeared on the detector. For this reason, the nanoparticles formed by solutions with pH 5 or 7 were the ones studied.

From the analysis on Figure 3.4, it was possible to observe that for longer times, 45 min, higher pH synthesis turned out in particles more heterogeneous in size (f). Figure 3.4 (d), a 15 min microwave synthesis, resulted in particles that did not have the required properties to pass on the detector. Some particles were measured once again, as represented in Table 3.2, confirming that the sizes were as expected, below 100 nm, and standard deviation was higher for higher pH. On top of these results, Caruso R., by a synthesizing ZrO_2 powders at different pHs, also

concluded that synthesis at pH 5 resulted in softer powders which helps when grinding the material in a later stage [94].

Table 3.2 – Size measurements of ZrO_2: 0.015 Yb3+ (NaOH) particles with different conditions.

(b) – ZrO2: Yb3+ (NaOH) pH 5, 25 min, 200 °C	83 ± 11 nm
(c) – ZrO2: Yb3+ (NaOH) pH 5, 45 min, 200 °C	81 ± 12 nm
(e) – ZrO2: Yb3+ (NaOH) pH 7, 25 min, 200 °C	88 ± 15 nm
(f) – ZrO2: Yb3+ (NaOH) pH 7, 45 min, 200 °C	95 ± 26 nm

From the results mentioned above, pH 5 was chosen over pH7 to continue the examination of the reagent NaOH.

As well as the most suitable pH, it was also possible to determine which time was the more indicated for the microwave synthesis. 15, 25, 45 and 90 min were the times tested. Considering production costs and the fact that more time in microwave induced higher particle size standard deviations, as seen above, 15 and 25 min were preferred and repeated more often. After carrying out several trials, it was possible to verify the consistency of the detector's response on the produced powders. All the 25 min synthesized powders passed green instead of 15 min, being this the main reason of choosing 25 min as the ideal time.

Temperature synthesis with reagent NaOH was the last analysis before moving to the next reagent, hexamethylenetetramine. Being the topic of this work low-cost nanomaterials, not only the materials used were cheaper, but a consistent attempt of using lower temperatures and decrease the amount of materials to get to the final goal was taking into account. This way, temperatures less than 200 °C were tried out.

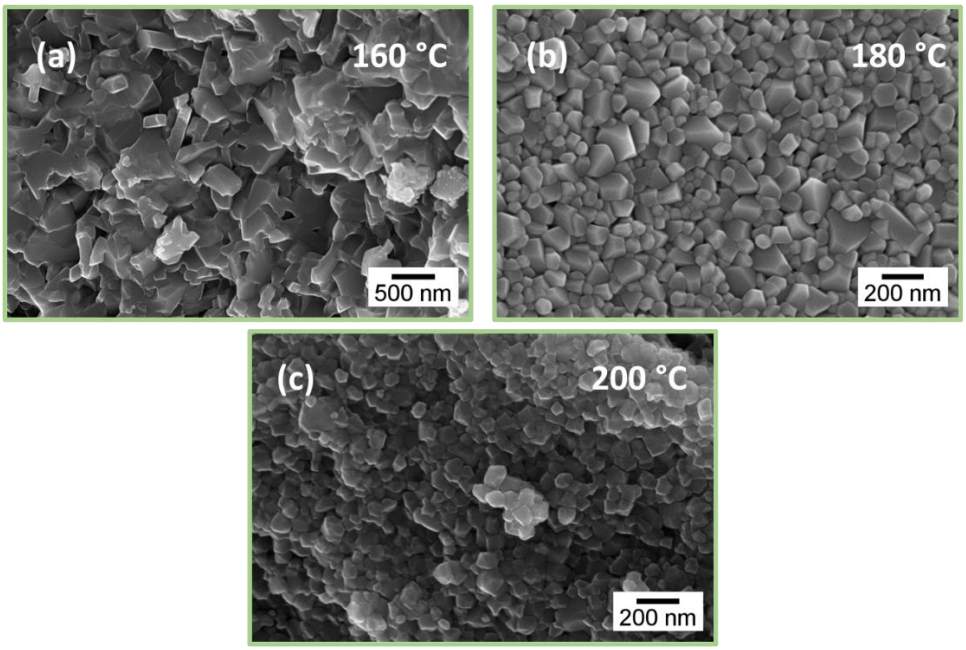

Figure 3.5 – SEM images of different synthesis temperatures of ZrO_2: 0.015 Yb3+ (NaOH) pH 5, 25 min synthesis. (a) 160 °C, (b) 180 °C, (c) 200 °C.

Analysing SEM images from Figure 3.5 and reminding the detector's response on the powders some conclusions were drawn. From the different temperatures tested, 140 ℃ was not considered since it did not pass on the detector. Figure 3.5 (a), that represents 160 ℃, can be observed that the process appears to be uncompleted as the particles were all combined and clustered. Measures could not be performed since the particles do not have a defined separated surface from each other. In (b) and (c) the outcome was not the same as it was possible to clearly see the limits/separation of each nanoparticle. From the measures done, presented in Table 3.3, it can be said that synthesis at 200 ℃ does not result in bigger particles when comparing to 180 ℃. In both images they present alike geometries, with flat surfaces. For that reason, the 180 ºC was selected from now on.

Table 3.3 – Size measurements of ZrO_2: 0.015 Yb3+ (NaOH) particles with different synthesis temperatures.

ZrO2: Yb3+ (NaOH) pH 5, 25 min, 180 ℃	94 ± 26 nm
ZrO2: Yb3+ (NaOH) pH 5, 25 min, 200 ℃	83 ± 11 nm

3.3 ZrO_2: Yb3+ (HMT)

3.3.1 Molar concentration and synthesis temperature

After concluding the tests with Sodium Hydroxide, it is presented in this subsection, nanoparticles synthesized with hexamethylenetetramine. Annealing temperatures (1000 ℃) and microwave time (25 min) were unchanged, testing now molar concentration of the new reagent and microwave temperature again. The concentrations analysed were 2, 25, 50 and 100 mM. Figure 3.6 represents SEM images from the achieved nanoparticles done at 180 ℃.

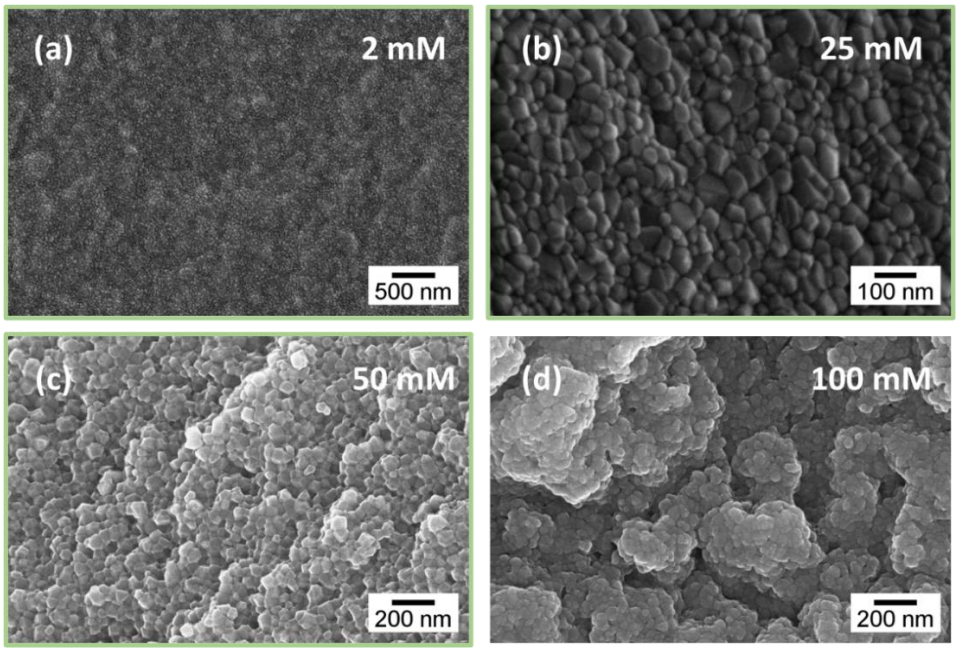

Figure 3.6 – SEM images of ZrO_2: 0.015 Yb3+ (HMT) with different concentrations. (a) 2 mM, (b) 25 mM, (c) 50 mM, (d) 100mM.

Some conclusions can be drawn from the above images. From Figure 3.6 (d) 100 mM powder besides not passing on the detector, also formed agglomerated clusters and seems to be melted, being a negative outcome, once a later objective was dispersion of the powder. Low concentrations turned out to have the qualities required to form looser nanoparticles and with the required optical properties to give green light on the detector. The particles of interest were measured as demonstrated in Table 3.4. Lower concentrations resulted in smaller particles, nevertheless did better when tried to grind. Both particles with 2 and 25 mM had similar size, but the concentration chosen was 25 mM.

Table 3.4 – Size measurements of ZrO_2: 0.015 Yb3+ (HMT) nanoparticles with different molar concentrations.

ZrO_2: Yb3+ ($C_6H_{12}N_4$) 2 mM, 25 min, 180 °C	46 ± 7 nm
ZrO_2: Yb3+ ($C_6H_{12}N_4$) 25 mM, 25 min, 180 °C	50 ± 9 nm
ZrO_2: Yb3+ ($C_6H_{12}N_4$) 50 mM, 25 min, 180 °C	61 ± 13 nm

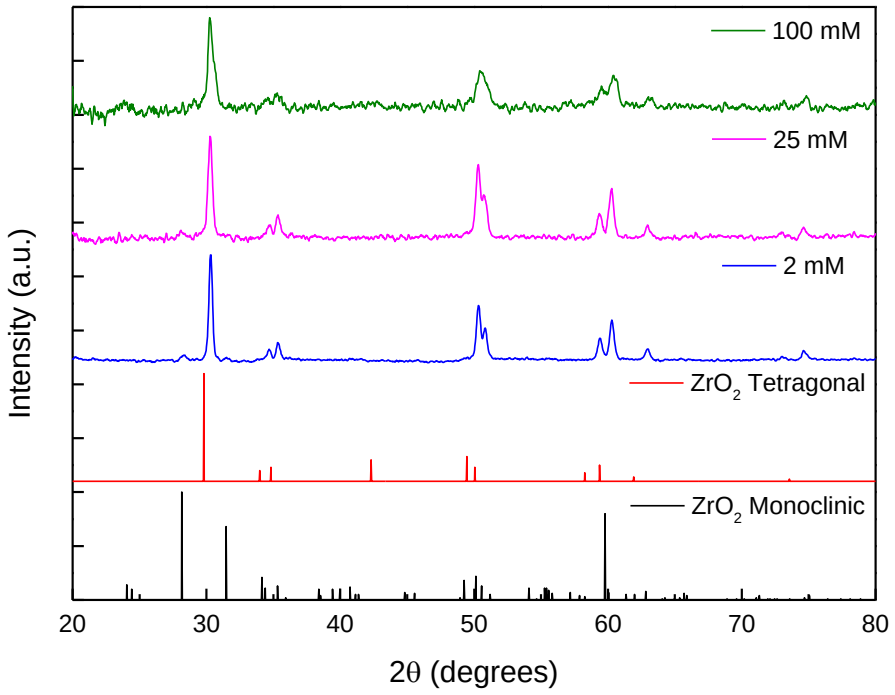

Figure 3.7 – XRD diffractograms of ZrO_2: 0.015 Yb3+ (HMT) with 3 different molar concentrations and standard data from JCPDS cards 37-1484 and 24-1164 (simulated ZrO_2 tetragonal and monoclinic phases). 2 mM, 25 mM and 100 mM.

An XRD analysis was also carried out to understand if any structural difference would be noticed, since only one concentration was giving a powder capable of passing on the detector. From the analysis of Figure 3.7, all concentrations turned out in the same ZrO_2 tetragonal phase. Peaks from the sample that was synthesized with 25 mM, represented a slight increase in crystallinity over the others concentrations. Tetragonal phase was achieved as the peaks at 2θ = 30.2°, 35.2°, 50.6° and 60.2° correspond to (101), (110), (112) and (211) planes that are characteristics of tetragonal phase of ZrO_2 [91].

The same study done with NaOH on the synthesis temperature was also carried out with HMT. After several synthesis using the 3 temperatures for this study, 160, 180 and 200 °C, but only particles done at 180 °C passed on the detector. It was recognized that the particles that show faceted structure always pass on the detector as seen in Figure 3.8 (b). In (c) the achieved particles, do not show loose particles, but a complete agglomerate, being the opposite of what was desired. Owing to this result, 180 °C was the temperature set for both reagents NaOH and HMT on the microwave synthesis.

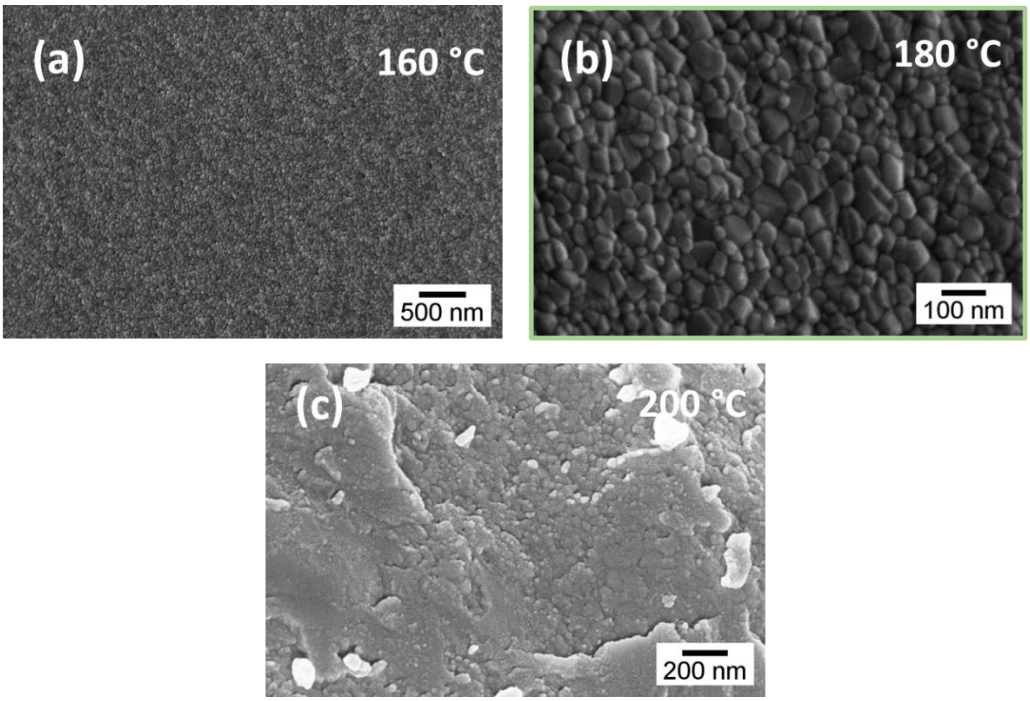

Figure 3.8 – SEM images of ZrO_2: 0.015 Yb3+ (HMT) with different synthesis temperatures. (a) 160 °C, (b) 180 °C, (c) 200 °C.

From the four reagents tested on this thesis, to achieve ZrO_2 nanoparticles that would match the properties analysed by the detector, only the two already presented worked, urea and ethylenediamine never worked and have been discarded. The creation of a replica nano-marker must, of necessity, fulfil the parameter of passing on the detector, otherwise it would have no use. Taking into account that both reagents urea and ethylenediamine never complied this factor, out of all experiments no results were shown regarding them. An average of all particles that were annealed at 1000 °C was calculated resulting in a mean of 75 ± 14 nm.

3.4 Replica nano-marker (ZrO_2:Yb3+)

Synthesis were concluded and the use of CEM Discover SP was replaced by CEM Mars One microwave, to understand if the scale up process could work. The conditions used were the same that gave better results in the last sections: 25 min at 180 °C microwave synthesis with posterior 1000 °C annealing. When using NaOH pH 5 was used and for the HMT, 25 mM. Due to some inconsistency from the reagent sodium hydroxide on validation by the detector and difficulty in grinding the powder (as presented in Figure 2.1), HMT was chosen for developing

the replica and developed nano-marker, ZrO_2:Yb3+ and ZrO_2:Yb3+/Er3+, respectively. From this point forward, only HMT was used for the microwave synthesis. The amount of dopant, 1.5 %, resulted from the mentioned work from Freire T., where different concentrations were tested and 1.5 % turned out to be the most suitable [92]

For the purpose of guaranteeing that the powder resultant from the Mars One microwave had the same structural and photoluminescent, tests were conducted comparing powders synthesized on both equipments.

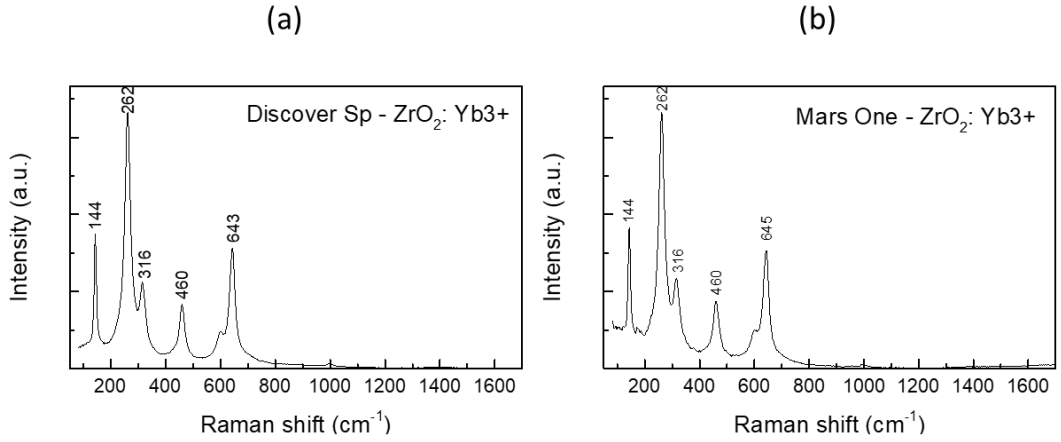

Figure 3.9 – Raman Spectroscopy of ZrO_2: 0.015 Yb3+ produced on both microwaves. (a) CEM Discover SP, (b) CEM Mars One.

Raman spectroscopy is a high-resolution photonic technique that can provide chemical and structural information for almost any material in just a few seconds. Quintard *et al* (2004), demonstrated that Raman Spectra of the Tetragonal Phases of Zirconia have peaks at 145 cm^{-1}, 264 cm^{-1}, 320 cm^{-1}, 460 cm^{-1}, 606 cm^{-1} and 641 cm^{-1} [95]. The peaks showed in graphs in Figure 3.9 allow a clear confirmation that the materials are the same, Zirconium Oxide with tetragonal phase. No peak belonging to other phase has been found.

The optical characterization of the nano-marker material has been carried out to assure that photoluminescent response was not altered when making the transition from one microwave to the other.

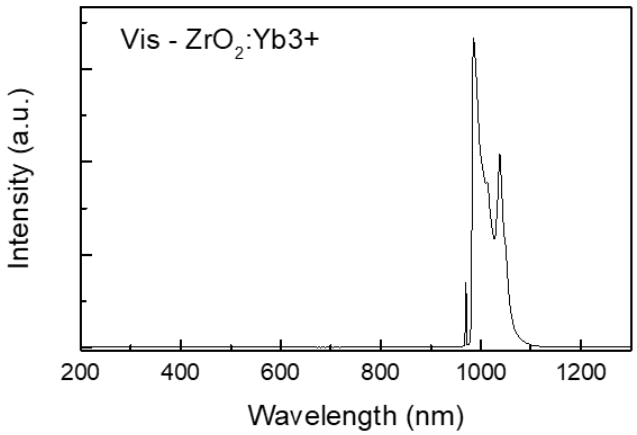

Figure 3.10 – Photoluminescence study on ZrO_2: 0.015 Yb3+ synthesized on CEM Discover SP. Visible band.

Figure 3.10 shows the visible emission spectra of the replica nano-marker. It is possible to observe that one band of emission referring to the Yb^{3+}, between 1000 and 1100 nm, where the peak at greater intensity is at 1037 nm associated to transitions from ($^2F_{5/2} \rightarrow {}^2F_{7/2}$) energy level [96,97]. The peak situated at 983 is from the laser incident on the sample. The spectrum from Figure 3.10 had the goal to confirm that no photoluminescent alterations occurred when changing equipments.

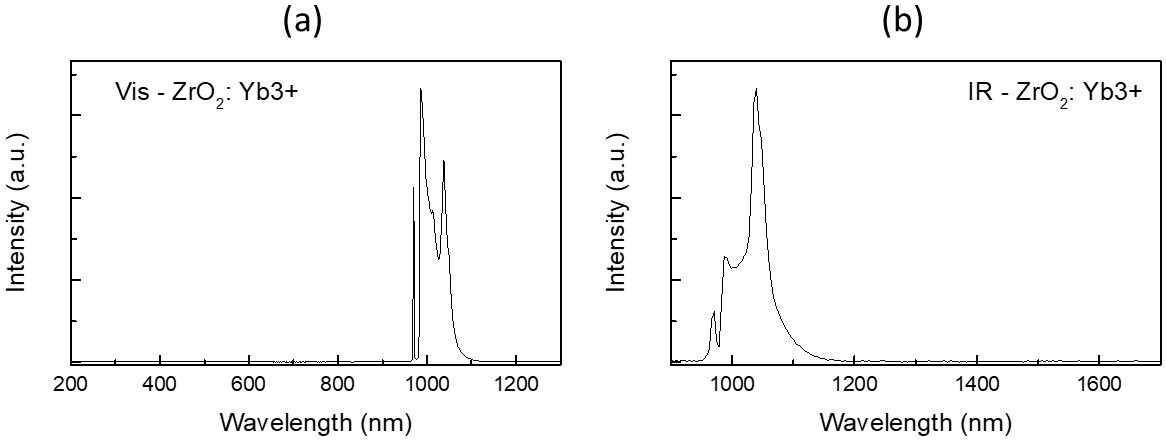

Figure 3.11 – Photoluminescence study on ZrO_2: 0.015 Yb3+ synthesized on CEM Mars One. (a) visible band, (b) infrared band.

As it is possible to observe in Figure 3.11, the same photoluminescent (PL) response was obtained, which led to confirm that the properties remained. No differences between both microwaves utilized has been found on the PL properties. With this study, it was concluded that the scale up process has been correctly achieved. This spectrum is an imitation of the one referring to the commercial nano-marker, demonstrating that it was possible to create a replica, what consequently shown an insecurity in the commercial product. To overcome this situation a solution, analysed ahead in this work, was the addition of a second dopant to the matrix, increasing the security of the nano-marker.

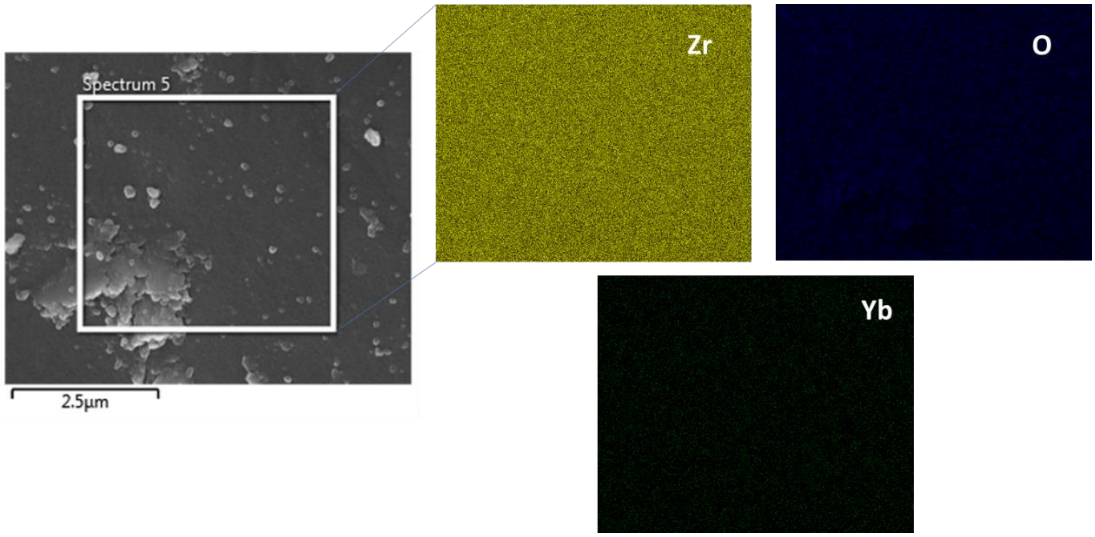

Figure 3.12 – SEM image (a) and EDS analysis of the replica nano-marker (ZrO_2: 0.015 Yb3+). The corresponding EDS maps for Zr, O and Yb are presented.

In order to analyse the distribution of all elements in the particles an EDS study was conducted. It can be observed in Figure 3.12 that there is a homogeneous distribution of all compounds. Zirconia and oxygen come from the matrix while Yb is the dopant. It was already expected low content of Yb, taking into account that only 1.5 % in molar concentration was used.

3.5 Ink Formulation

The next goal on the project was to disperse this powder on the white ink provided by INCM turning it into security ink. Some attempts were carried out using Triton and PVP but all the results were the same in the way that all alternatives turned into successful dispersions. Because the simplest way is the best and cheapest way, no dispersant was used. The security ink was tested 3 weeks later to assure stability (no sedimentation) and again, the response was positive, tag08.

A number of trials of powder/ink proportion was done, by mixing powder and ink followed by a manual spread on a paper using a spatula. After every spread on paper an UV cure for 10 min was carried out. Every trial passed on the detector, from 1:2 to 1:500 (Figure 3.15). The more percentage in powder the greyer the ink would become.

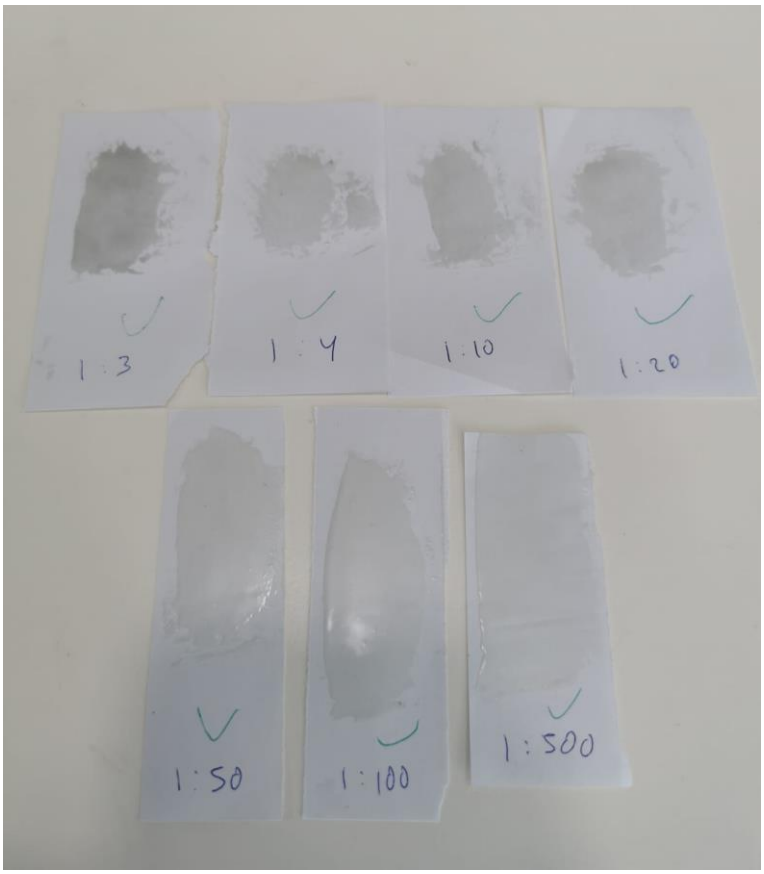

Figure 3.13 – Different proportions of powder/ink.

The materials presented on Figure 3.13 were also analysed with SEM, with the intent to understand how the particles were dispersed within the ink. A sample with only ink (blank ink) is represented in Figure 3.14 (a), together with three different proportions, 1:2, 1:50 and 1:500. The white dots seen in all images do not represent the produced powder, since (a) also shows the same characteristic. The pattern created in the ink is not uniform. It was not possible to effectively distinguish the particles inside the ink.

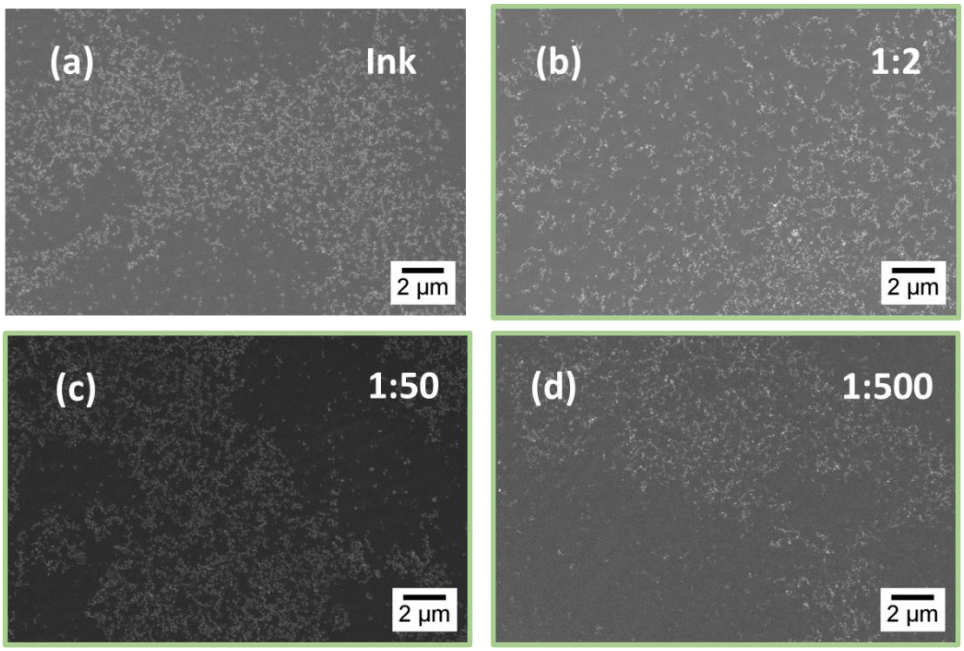

Figure 3.14 – SEM images of different proportions of powder/ink. (a) 1:2, (b) 1:50, (c) 1:500.

To test the printing methods the ratio chosen was 1:100 powder/ink in order to use low quantity of powder reducing costs and at the same time to safely maintain the photoluminescent properties.

3.6 Printing Techniques

On this present year the whole world had to face a new way of living and new security measures due to the pandemic Covid-19. One of the most noticeable effects on the population was the number of establishments closed for an indefinite period of time such as INCM. The most important printing technique should have been offset, as it is the one used in INCM. Since it was not possible to go there and try out this technique, two possible alternatives were implemented in the Cenimat facilities – Screen printing and flexographic (same principle as offset) printing. The ink used in this section is a mix of the produced nano-marker ZrO_2: Yb3+ and the provided white ink with a ratio 1:100 and it will be called replica ink.

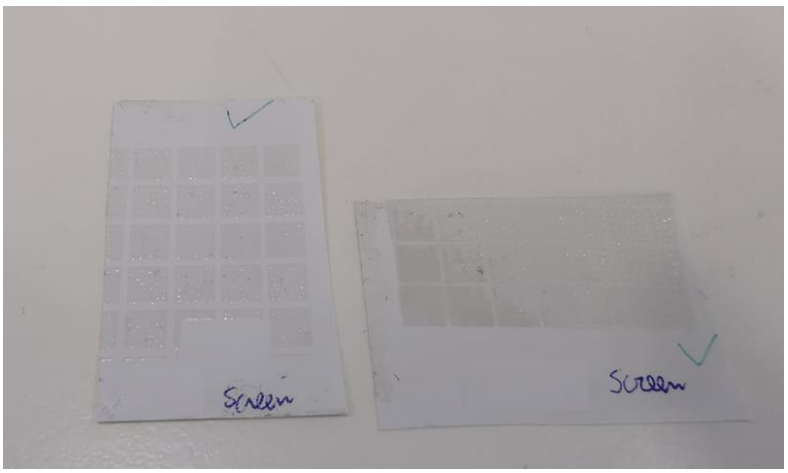

Figure 3.15 – Replica security ink printed by screen printing.

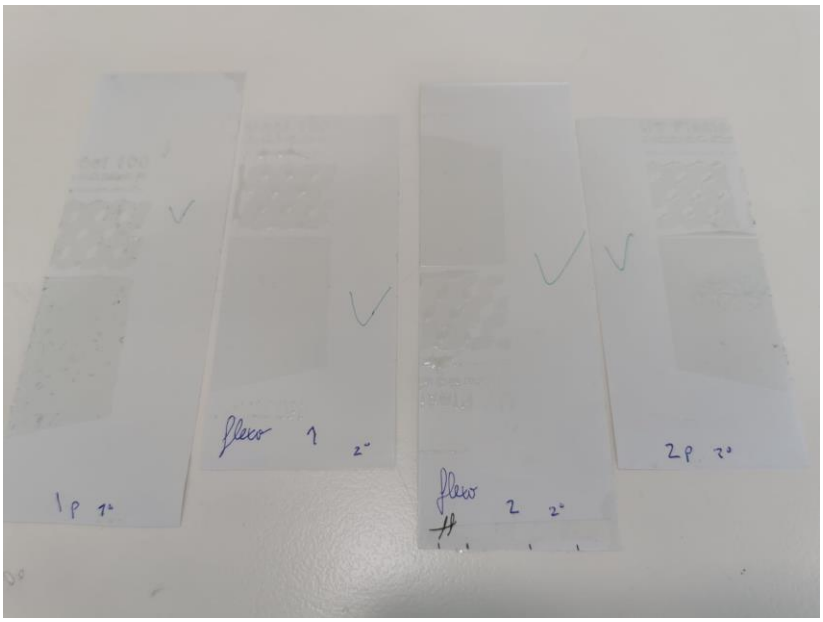

Figure 3.16 - Replica security ink printed by flexographic. Two trials were done with two different parameters.

Both figures above represent the positive results of the printing methods. Figure 3.15 shows both trials of screen printing and Figure 3.16 the two setups tried. Two different pairs of pressure were used – 1st 40 for the substrate and 2nd 70 for anilox and then 80 for the substrate and 40 for anilox. The values of the average thicknesses of the layers can be seen in Table 3.5. The aim for these tests was to confirm that the particles would maintain the dispersive properties and would not agglomerate when passing through the screen mesh and the anilox on both techniques. All the samples tested successfully passed on the detector. Moreover, it was identified that all the screen and flexo setup could be cleaned just with ethanol instead of the solvent used in INCM which is highly inflammable and toxic.

Table 3.5 – Thickness of printed layers by screen and flexo printing, measured with a profilometer.

Screen 1st trial	17 ± 6 µm
Screen 2nd trial	25 ± 8 µm
Flexo 1st setup 1st trial	13 ± 10 µm
Flexo 1st setup 2nd trial	14 ± 2 µm
Flexo 2nd setup 1st trial	12 ± 1 µm
Flexo 2nd setup 2nd trial	10 ± 3 µm

The noticeable characteristic at this point was that the thinnest layer was not yet achieved. It is possible to have thinner layers (as thin as the detector still validates), saving more material per print and also increase the security as it is harder to discover the layer on the product.

3.7 Developed nano-marker

Having the first and most important objective of this work finished was time to go further in the investigation. The replica ink has come as an alternative to replace the existent one, once it is done with cheaper materials. In this section it is presented a developed nano-marker which its main feature when comparing to the replica is an increase of security. Instead of one dopant, a second was introduced into the structure altering the photoluminescent response and a need of a new detector. The synthesis of this nanoparticles was done with the same parameters as the replica: 25 min at 180 °C on CEM Mars One microwave. For each 100 ml of solution 25 mM of HMT was used, but this time the amounts of dopants were 10 % mol Yb and 1.625 % mol Er. The same studies done on the replica nano-marker were carried out on the developed nano-marker.

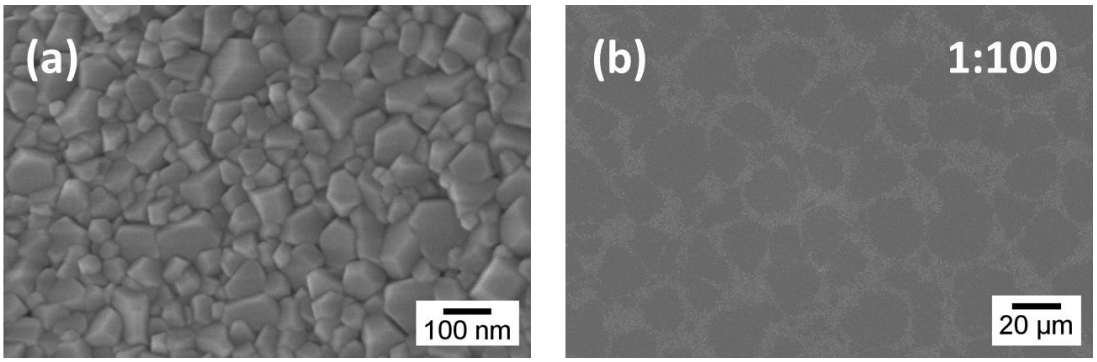

Figure 3.17 – SEM images of ZrO_2: 0.1 Yb3+/ 0.01625 Er3+. (a) particles, (b) developed ink.

Figure 3.17 represents both the particles and respective developed ink. From (a) it can be seen that the particles are not uniform in shape or size, but most important did not exceeded 100 nm. It is also noticeable that they show faceted morphology as the developed marked. Table 3.6 shows an average of the particles in question. The size deviation (31 nm) is higher than the ZrO_2: Yb3+ nanoparticles (14 nm). The same heterogeneous pattern can be observed on the developed ink as it was expected. Only a small percentage of the material present on Figure 3.17 (b) is produced powder not affecting the microscopic forms produced by the ink.

Table 3.6 – Size measurements of developed nano-marker (ZrO_2: 0.1 Yb3+/ 0.01625Er3+) particles.

ZrO_2:Yb3+/Er3+	78 ± 31 nm

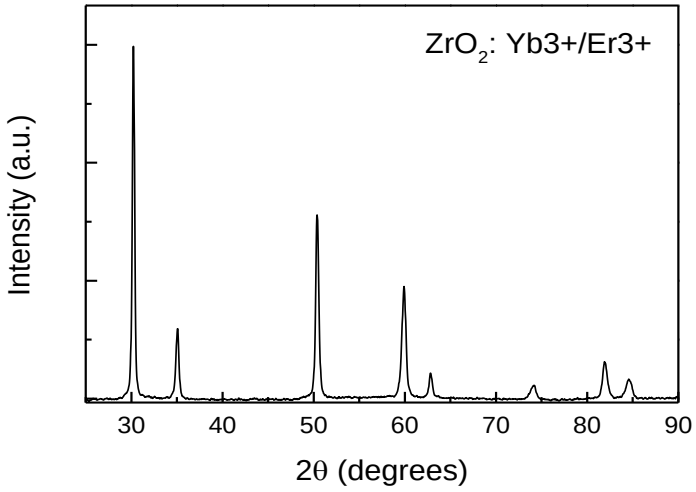

Figure 3.18 – XRD diffractogram of ZrO_2: 0.1 Yb3+/ 0.01625 Er3+ powder.

A structural analysis is present on Figure 3.18 confirming that a crystalline structure is present. The present phase is tetragonal phase, in the same way that was present for the replica nano-marker. Peaks at 2θ = 30.2°, 35.2°, 50.6° and 60.2° correspond to (101), (110), (112) and (211) planes that are characteristics of tetragonal phase [91]. No peaks from other phases were present in the sample.

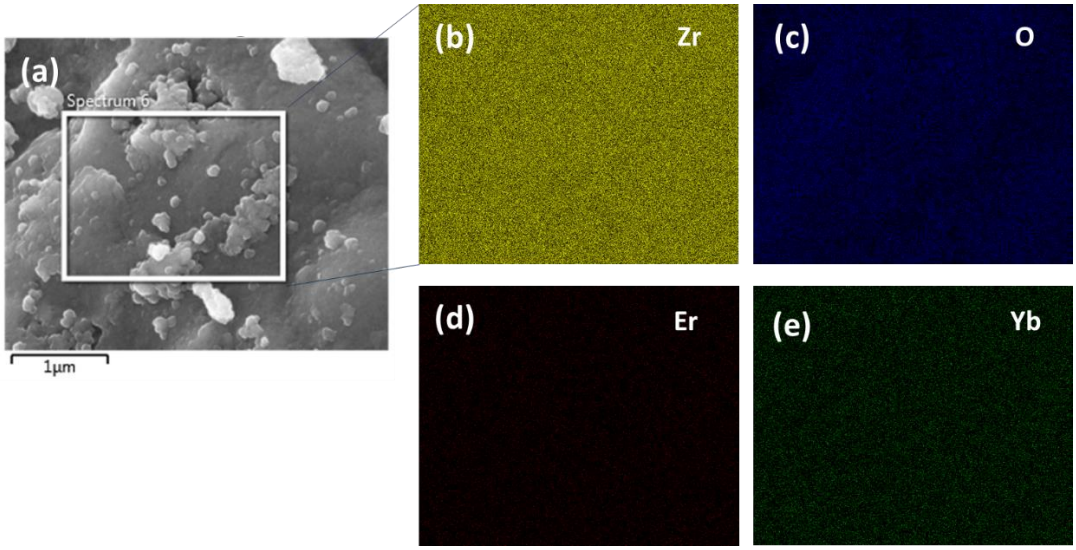

Figure 3.19 – SEM image (a) and EDS analysis of the developed nano-marker (ZrO_2: Yb3+/Er3+). The corresponding EDS maps for Zr, O, Er and Yb are presented.

An EDS analysis was carried out to assure the presence of both dopants in the particles. As Figure 3.19 suggests both dopants are present, but their intensities are different. The amount of Yb used in the synthesis was close to 10 times as the Er. From the analysis, 14.3% was Yb and 1.7% Er. The greater presence of Yb meets the expected results. Both Oxygen and Zirconia come from the matrix of the developed nanoparticles.

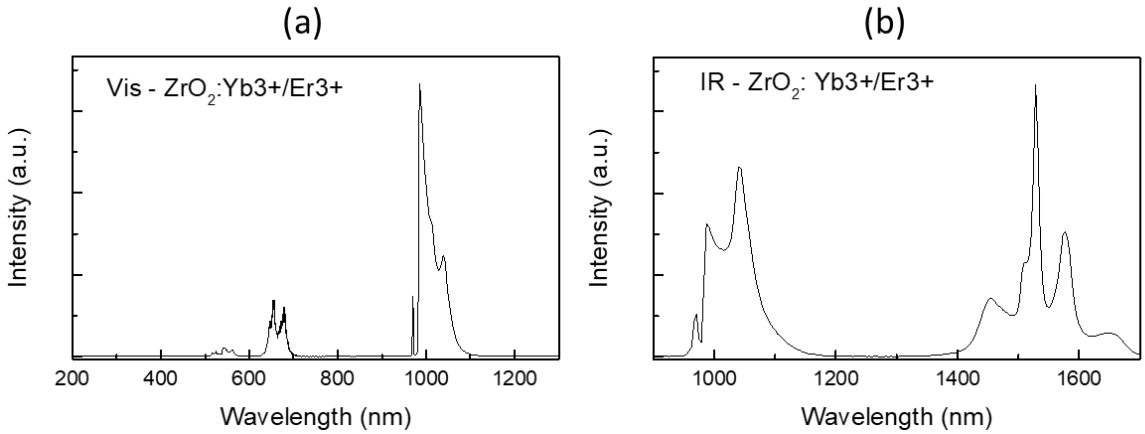

Figure 3.20 – Photoluminescence study on ZrO_2: Yb3+/Er3+ synthesized on CEM Mars One. (a) visible band, (b) infrared band.

The last analysis was the one that it is possible to demonstrate the most important advantage of this developed nano-marker. In Figure 3.20 the photoluminescent test clearly shows not only the emission peak of Yb3+ between 1000 and 1100 nm, as seen in Figure 3.10 and 3.11, but other emission peaks as well. The peak observed between 1400 and 1700 nm, with the peak of greater intensity at 1530 nm seen in infrared band (b), refers to Er3+. When looking to the visible band, the peak seen between 600 and 700 nm, is a result of the combination of Yb3+ and Er 3+ emission. The red emission band at around 660 nm is assigned to the ($^4F_{9/2} \rightarrow {}^4I_{15/2}$) intra-4f transitions of Er3+ [43,98]. Er3+ ions have a low-absorption cross section, but due to spectral overlap between Yb3+ emission ($^2F_{7/2} \rightarrow {}^2F_{5/2}$) and Er3+ absorption ($^4I_{15/2} \rightarrow {}^4I_{13/2}$) results in an efficient resonant energy transfer from Yb3+ to Er3+ in co-doped system [12,45,99].

Another emission band is characteristic from Er3+/Yb3+ combination at 520-550 nm. It is the second most intense photoluminescent band when these 2 rare earth elements are combined [43]. In Figure 3.20 (a) is possible to see a small intensity around 500 to 600 nm but not comparable as the red band.

The upconversion process occurred, once lower energy photons (980 nm wavelength incident laser) excited higher energy state photons (visible light peaks). The correspondent colour of peaks situated in 600-700 nm wavelength is reddish orange. Figure 3.21 is a photography taken to the developed nano-powder when irradiated by the 980 nm wavelength laser. The colour observed matches the reddish orange, as expected.

Figure 3.21 – Real image of upconversion process on the developed nano-marker.

The use of the developed nano-marker did not come alone, as it is necessary to test it, the same way the replica was. Unfortunately, the corresponding developed detector was not ready, incapacitating the test of the developed nanoparticles and ink.

This work brought great expectations for future improvements on security inks. On the one hand, saving resources on finding cheaper materials to replace the ones that already exist allows that more products contain this safety property. On the other hand, it has been developed a new marker, with another level of security. By using two dopants in the developed nano-marker, it is possible to manipulate the intensity of the luminescent peaks. This manipulation of intensities is what makes the developed nano-marker more secure than the commercial one.

4 Conclusion

The present work was centered on the production of a new nano-marker based on zirconia oxides doped with rare earth dopants, such as ytterbium and erbium. This marker was incorporated in inks transforming them into security inks. The work was in fact successful and the final objective, which consisted on printing security inks on specific substrates, was achieved. This type of inks already exists and are commonly used in some specific security applications. This time, a new material was studied and has been concluded that it works in the same way bringing some benefits.

Through a simple and environmentally friendly microwave synthesis zirconia oxides nanoparticles were grown with four different reagents, giving a special attention to NaOH and Hexamethylenetetramine. These two materials worked effectively in the synthesis, as they helped to achieve the desired nanoparticles with a maximum of 100 nm. Due to the stability of the powder in the ink, it was not necessary the addition of another material for dispersing purposes, a manual mixing of the powder into the ink was enough. Besides the two printing techniques used in this work, flexo and screen printing, have resulted it is of great interest to test on offset. It is expected that it will work as the setup is very similar to flexography.

First of all, cheaper and more abundant materials were used to conceive the replica security ink, secondly, as it was shown, it was only required just a small amount of marker to give the ink its required luminescent properties. For these two reasons it is possible to produce large amounts of ink, enhancing the alternative of using more frequently this security method in a more abundant way. INCM could increase the security in a wide range of more products that need authentication due to the ease of application of this safety measure.

It has not been carried out a more detailed studied regarding the developed nano-marker since the developed detector had some problems and was not able to test samples. Also, accelerating aging, photoluminescent and other stability tests, for instance zeta potential, would be of quite interest for further confirmation of properties of the security inks done in this work. The lack of mobility and above all, physical social distancing, due to the covid-19 pandemic has affect the later stages of the thesis for the tests that were still undone.

Finally, it would be of great interest to study and realize how these nano-markers would respond if mixed with coloured inks, opening a new possibility of security hiding the marker under any surface.

5 References

[1] Counterfeit Coins: The World's 2nd Oldest Profession n.d. https://www.texmetals.com/news/counterfeit-coins-the-worlds-2nd-oldest-profession (accessed December 1, 2020).

[2] Shell M. Wampum and the Origins of American Money. 2013.

[3] Bian X, Veloutsou C, Roll M, Veloutsou C, Prendergast G, Chuen LH, et al. Non-Deceptive Counterfeiting Purchase Behavior : Antecedents Of Attitudes And ... ProQuest Dissertations and Theses 2002;14:127–37.

[4] Vida I. Determinants of Consumer Willingness to Purchase Non-Deceptive Counterfeit Products and the European Union. Managing Global Transitions 2007;3:253–70.

[5] Wood L. Global Brand Counterfeiting Report 2018-2020 - ResearchAndMarkets.com. AP News 2018. https://apnews.com/ef15478fa38649b5ba29b434c8e87c94.

[6] Frontier Economics. THE ECONOMIC IMPACTS OF Report prepared for BASCAP and INTA. 2016.

[7] Orecchini G, Alimenti F, Palazzari V, Rida A, Tentzeris MM, Roselli L. Design and fabrication of ultra-low cost radio frequency identification antennas and tags exploiting paper substrates and inkjet printing technology. IET Microwaves, Antennas and Propagation 2011;5:993–1001. https://doi.org/10.1049/iet-map.2010.0344.

[8] Wang Y, Xu S, Lin J. Nuclear track anti-counterfeiting technique and its application in secure ID 2008;43:2006–8. https://doi.org/10.1016/j.radmeas.2008.04.024.

[9] Aggarwal AK, Kaura SK, Chhachhia DP, Sharma AK. Concealed moiré pattern encoded security holograms readable by a key hologram. Optics and Laser Technology 2006;38:117–21. https://doi.org/10.1016/j.optlastec.2004.10.010.

[10] Singh AK, Singh S, Gupta BK. Highly Efficient, Chemically Stable, and UV/Blue-Light-Excitable Biluminescent Security Ink to Combat Counterfeiting. ACS Applied Materials and Interfaces 2018;10:44570–5. https://doi.org/10.1021/acsami.8b18997.

[11] Meruga JM, Cross WM, Stanley May P, Luu Q, Crawford GA, Kellar JJ. Security printing of covert quick response codes using upconverting nanoparticle inks. Nanotechnology 2012;23. https://doi.org/10.1088/0957-4484/23/39/395201.

[12] Yao W, Tian Q, Liu J, Wu Z, Cui S, Ding J, et al. Large-scale synthesis and screen printing of upconversion hexagonal-phase NaYF4:Yb3+,Tm3+/Er3+/Eu3+ plates for security applications. Journal of Materials Chemistry C 2016;4:6327–35. https://doi.org/10.1039/c6tc01513a.

[13] Helmenstine AM. Pigment Definition and Chemistry n.d. https://www.thoughtco.com/pigment-definition-4141440 (accessed April 25, 2020).

[14] Microtrace. TAGGANTS ARE PART OF A STRONG BRAND-PROTECTION SOLUTION n.d. https://www.microtracesolutions.com/taggant-technologies (accessed March 20, 2020).

[15] Appaiah M. How Counterfeit Products Affect Brands and Consumers. Entrepreneur India n.d.

[16] Bradley S. Van Gosen, Philip L. Verplanck, Robert R. Seal II KRL, Gambogi and J. Rare-Earth Elements Chapter O of Critical Mineral Resources of the United States — Economic and Environmental Geology and Prospects for Future Supply Professional Paper 1802 – O U . S . Department of the Interior 2013.

[17] Lu Q, Hou Y, Tang A, Lu Y, Lv L, Teng F. Controlled synthesis and defect dependent upconversion luminescence of Y2O3: Yb, Er nanoparticles. Journal of Applied Physics 2014;115:1–5. https://doi.org/10.1063/1.4866054.

[18] Gupta BK, Haranath D, Saini S, Singh VN, Shanker V. Synthesis and characterization of ultra-fine Y2O 3:Eu3+ nanophosphors for luminescent security ink applications. Nanotechnology 2010;21. https://doi.org/10.1088/0957-4484/21/5/055607.

[19] Blumenthal T, Meruga J, Stanley May P, Kellar J, Cross W, Ankireddy K, et al. Patterned direct-write and screen-printing of NIR-to-visible upconverting inks for security applications. Nanotechnology 2012;23. https://doi.org/10.1088/0957-4484/23/18/185305.

[20] You M, Zhong J, Hong Y, Duan Z, Lin M, Xu F. Inkjet printing of upconversion nanoparticles for anti-counterfeit applications. Nanoscale 2015;7:4423–31. https://doi.org/10.1039/c4nr06944g.

[21] Meruga JM, Baride A, Cross W, Kellar JJ, May PS. Red-green-blue printing using luminescence-upconversion inks. Journal of Materials Chemistry C 2014;2:2221–7. https://doi.org/10.1039/c3tc32233e.

[22] Anderson DL. Chemical Composition of the Mantle 1983.

[23] B D, Scheers CL. ZIRCONIUM METAL, ITS MANUFACTURE, FABRICATION AND PROPERTIES 1945.

[24] Duwez POL, Brown FH, Odell F. The Zirconia-Yttria System n.d.

[25] Zhou B, Shi B, Jin D, Liu X. Controlling upconversion nanocrystals for emerging applications. Nature Nanotechnology 2015;10:924–36. https://doi.org/10.1038/nnano.2015.251.

[26] Weingarten DH, Lacount MD, van de Lagemaat J, Rumbles G, Lusk MT, Shaheen SE. Experimental demonstration of photon upconversion via cooperative energy pooling. Nature Communications 2017;8:1–7. https://doi.org/10.1038/ncomms14808.

[27] Technological Applications of Colour Chemistry. n.d.

[28] Lakowicz, Joseph R. Principles of Fluorescence Spectroscopy. n.d.

[29] Albani JR. Structure and Dynamics of Macromolecules: Absorption and Fluorescence Studies. n.d.

[30] Auzel F. Upconversion and Anti-Stokes Processes with f and d Ions in Solids. Chemical Reviews 2004;104:139–73. https://doi.org/10.1021/cr020357g.

[31] Hiraoka K. Fundamentals of Mass Spectrometry n.d.

[32] Bearden T. Anti-Stokes Emission Always Outputs More Energy than the Operator Inputs n.d. http://www.cheniere.org/misc/antistokes.htm (accessed April 5, 2020).

[33] Tian G, Zhang X, Gu Z, Zhao Y. Recent Advances in Upconversion Nanoparticles-Based Multifunctional Nanocomposites for Combined Cancer Therapy. Advanced Materials 2015;27:7692–712. https://doi.org/10.1002/adma.201503280.

[34] Smith KC. The Science of Photobiology. n.d.

[35] Michael K. Characterization of electronic transitions in complex molecules. Discussions of the Faraday Society 1950;9:14–9.

[36] Frazer L. Photochemical Upconversion Light Emitting Diode (LED): Theory of Triplet Annihilation Enhanced by a Cavity. Advanced Theory and Simulations 2019;2:1–10. https://doi.org/10.1002/adts.201800099.

[37] Baluschev S, Yakutkin V, Wegner G, Miteva T, Nelles G, Yasuda A, et al. Upconversion with ultrabroad excitation band: Simultaneous use of two sensitizers. Applied Physics Letters 2007;90:2005–8. https://doi.org/10.1063/1.2734475.

[38] Gholizadeh EM, Frazer L, MacQueen RW, Gallaher JK, Schmidt TW. Photochemical upconversion is suppressed by high concentrations of molecular sensitizers. Physical Chemistry Chemical Physics 2018;20:19500–6. https://doi.org/10.1039/c8cp02650e.

[39] Patra A, Friend CS, Kapoor R, Prasad PN. Fluorescence upconversion properties of Er3+-doped TiO 2 and BaTiO3 nanocrystallites. Chemistry of Materials 2003;15:3650–5. https://doi.org/10.1021/cm020897u.

[40] Joubert MF. Photon avalanche upconversion in rare earth laser materials. Optical Materials 1999;11:181–203. https://doi.org/10.1016/S0925-3467(98)00043-3.

[41] Paquin F, Rivnay J, Salleo A, Stingelin N, Silva C. Multi-phase semicrystalline microstructures drive exciton dissociation in neat plastic semiconductors. J Mater Chem C 2015;3:10715–22. https://doi.org/10.1039/b000000x.

[42] Shang Y, Hao S, Yang C, Chen G. Enhancing solar cell efficiency using photon upconversion materials. Nanomaterials 2015;5:1782–809. https://doi.org/10.3390/nano5041782.

[43] Singh AK, Kumar K, Pandey AC, Parkash O, Rai SB, Kumar D. Photon avalanche upconversion and pump power studies in LaF 3:Er3+/Yb3+ phosphor. Applied Physics B: Lasers and Optics 2011;104:1035–41. https://doi.org/10.1007/s00340-011-4673-2.

[44] Lavín V, Lahoz F, Martín IR, Rodríguez-Mendoza UR, Cáceres JM. Infrared-to-visible photon avalanche upconversion dynamics in Ho 3+-doped fluorozirconate glasses at room temperature. Optical Materials 2005;27:1754–61. https://doi.org/10.1016/j.optmat.2004.11.046.

[45] Li L, Wei X, Chen Y, Guo C, Yin M. Energy transfer in Tb3+,Yb3+ codoped Lu 2O3 near-infrared downconversion nanophosphors. Journal of Rare Earths 2012;30:197–201. https://doi.org/10.1016/S1002-0721(12)60022-2.

[46] Wang F, Banerjee D, Liu Y, Chen X, Liu X. Upconversion nanoparticles in biological labeling, imaging, and therapy. Analyst 2010;135:1839–54. https://doi.org/10.1039/c0an00144a.

[47] Mahata MK, Hofsäss HC, Vetter U. Photon-Upconverting Materials: Advances and Prospects for Various Emerging Applications. Luminescence - An Outlook on the Phenomena and Their Applications 2016. https://doi.org/10.5772/65118.

[48] Chen G, Qiu H, Prasad PN, Chen X. Upconversion nanoparticles: Design, nanochemistry, and applications in Theranostics. Chemical Reviews 2014;114:5161–214. https://doi.org/10.1021/cr400425h.

[49] Sedlmeier A, Achatz DE, Fischer LH, Gorris HH, Wolfbeis OS. Photon upconverting nanoparticles for luminescent sensing of temperature. Nanoscale 2012;4:7090–6. https://doi.org/10.1039/c2nr32314a.

[50] Wang C, Tao H, Cheng L, Liu Z. Near-infrared light induced in vivo photodynamic therapy of cancer based on upconversion nanoparticles. Biomaterials 2011;32:6145–54. https://doi.org/10.1016/j.biomaterials.2011.05.007.

[51] Hu Y, Shao Q, Dong Y, Jiang J. Energy loss mechanism of upconversion core/shell nanocrystals. Journal of Physical Chemistry C 2019;123:22674–9. https://doi.org/10.1021/acs.jpcc.9b07176.

[52] Ochiai E-I. General Principles of Biochemistry of the Elements. 1987.

[53] What are “rare earths” used for? n.d. https://www.bbc.com/news/world-17357863 (accessed May 10, 2020).

[54] Gupta BK, Haranath D, Saini S, Singh VN, Shanker V. Synthesis and characterization of ultra-fine Y2O 3:Eu3+ nanophosphors for luminescent security ink applications. Nanotechnology 2010;21. https://doi.org/10.1088/0957-4484/21/5/055607.

[55] Charalampides G, Vatalis KI, Apostoplos B, Ploutarch-Nikolas B. Rare Earth Elements: Industrial Applications and Economic Dependency of Europe. Procedia Economics and Finance 2015;24:126–35. https://doi.org/10.1016/s2212-5671(15)00630-9.

[56] Jha AR. Rare Earth Materials: Properties and Applications. 2014.

[57] Xiantao W, Jiangbo Z, Weiping Z, Yong L, Min Y. Cooperative energy transfer in Eu3+, Yb3+ codoped Y2O3 phosphor. Journal of Rare Earths 2010;28:166–70. https://doi.org/10.1016/S1002-0721(09)60073-9.

[58] Sun LD, Dong H, Zhang PZ, Yan CH. Upconversion of rare earth nanomaterials. Annual Review of Physical Chemistry 2015;66:619–42. https://doi.org/10.1146/annurev-physchem-040214-121344.

[59] Chen GY, Zhang YG, Somesfalean G, Zhang ZG, Sun Q, Wang FP. Two-color upconversion in rare-earth-ion-doped ZrO2 nanocrystals. Applied Physics Letters 2006;89:1–4. https://doi.org/10.1063/1.2363146.

[60] de La Rosa-Cruz E, Díaz-Torres LA, Rodríguez-Rojas RA, Meneses-Nava MA, Barbosa-García O, Salas P. Luminescence and visible upconversion in nanocrystalline ZrO2:Er3+. Applied Physics Letters 2003;83:4903–5. https://doi.org/10.1063/1.1632020.

[61] Meza O, Diaz-Torres LA, Salas P, de La Rosa E, Solis. D. Color tunability of the upconversion emission in Er-Yb doped the wide band gap nanophosphors ZrO2 and Y2O3. Materials Science and Engineering B: Solid-State Materials for Advanced Technology 2010;174:177–81. https://doi.org/10.1016/j.mseb.2010.03.015.

[62] Wang H, Liu YB, Kong LW. Simple and eco-friendly hydrothermal synthesis of luminescent carbon nanoparticles for H2O2 detection. Advanced Materials Research 2014;997:791–4. https://doi.org/10.4028/www.scientific.net/AMR.997.791.

[63] Kim Y il, Kim D, Lee CS. Synthesis and characterization of CoFe2O4 magnetic nanoparticles prepared by temperature-controlled coprecipitation method. Physica B: Condensed Matter 2003;337:42–51. https://doi.org/10.1016/S0921-4526(03)00322-3.

[64] Cruz LS, Sciena CR, Correa DS, Paris EC. Síntese Por Coprecipitação De Nanopartículas De Hidroxiapatita E Óxido Cúprico Para Aplicação No Agronegócio. Simpósio Nacional de Instrumentação Agropecuária 2014:439–42.

[65] Patterson JW. Coprecipitation. Environmental Encyclopedia n.d. https://www.encyclopedia.com/environment/encyclopedias-almanacs-transcripts-and-maps/coprecipitation.

[66] Patnaik P. Dean's analytical chemistry handbook. 2004.

[67] Hench LL, West JK. The Sol-Gel Process. Chemical Reviews 1990;90:33–72. https://doi.org/10.1021/cr00099a003.

[68] Benvenutti E v., Moro CC, Costa TMH, Gallas MR. Materiais híbridos à base de sílica obtidos pelo método sol-gel. Quimica Nova 2009;32:1926–33. https://doi.org/10.1590/S0100-40422009000700039.

[69] Mirzaei A, Neri G. Microwave-assisted synthesis of metal oxide nanostructures for gas sensing application: A review. Sensors and Actuators, B: Chemical 2016;237:749–75. https://doi.org/10.1016/j.snb.2016.06.114.

[70] Comparing Microwave to Conventional Heating & Drying 2012. https://www.manufacturing.net/home/article/13149658/comparing-microwave-to-conventional-heating-drying.

[71] Grewal AS. Microwave assisted synthesis: a green chemistry approach 2013. https://www.researchgate.net/figure/Comparison-of-microwave-heating-versus-conventional-heating-18_fig1_261872979.

[72] Imran M, Riaz S, Sanaullah I, Khan U, Sabri AN, Naseem S. Microwave assisted synthesis and antimicrobial activity of Fe 3 O 4 -doped ZrO 2 nanoparticles. Ceramics International 2019;45:10106–13. https://doi.org/10.1016/j.ceramint.2019.02.057.

[73] Bondioli F, Leonelli C, Manfredini T, Ferrari AM, Caracoche MC, Rivas PC, et al. Microwave-hydrothermal synthesis and hyperfine characterization of praseodymium-doped nanometric zirconia powders. Journal of the American Ceramic Society 2005;88:633–8. https://doi.org/10.1111/j.1551-2916.2005.00093.x.

[74] Gnanamoorthi K, Balakrishnan M, Mariappan R, Ranjith Kumar E. Effect of Ce doping on microstructural, morphological and optical properties of ZrO2 nanoparticles. Materials Science in Semiconductor Processing 2015;30:518–26. https://doi.org/10.1016/j.mssp.2014.10.054.

[75] Opalinska A, Leonelli C, Lojkowski W, Pielaszek R, Grzanka E, Chudoba T, et al. Effect of pressure on synthesis of Pr-doped Zirconia powders produced by microwave-driven hydrothermal reaction. Journal of Nanomaterials 2006;2006:1–8. https://doi.org/10.1155/JNM/2006/98769.

[76] Smits K, Jankovica D, Sarakovskis A, Millers D. Up-conversion luminescence dependence on structure in zirconia nanocrystals. Optical Materials 2013;35. https://doi.org/10.1016/j.optmat.2012.09.038.

[77] Gayatri Sharma K, Shanta Singh N, Rangeela Devi Y, Rajmuhon Singh N, Dorendrajit Singh S. Effects of annealing on luminescence of CaWO4:Eu3+ nanoparticles and its thermoluminescence study. Journal of Alloys and Compounds 2013;556:94–101. https://doi.org/10.1016/j.jallcom.2012.12.087.

[78] Vogelsang J, Brazard J, Adachi T, Bolinger JC, Barbara PF. Watching the annealing process one polymer chain at a time. Angewandte Chemie - International Edition 2011;50. https://doi.org/10.1002/anie.201007084.

[79] Gauna MR, Conconi MS, Gomez S, Suárez G, Aglietti EF, Rendtorff NM. Monoclinic-tetragonal zirconia quantification of commercial nanopowder mixtures by XRD and DTA. Ceramics - Silikaty 2015;50.

[80] Djurado E, Bouvier P, Lucazeau G. Crystallite size effect on the tetragonal-monoclinic transition of undoped nanocrystalline zirconia studied by XRD and Raman spectrometry. Journal of Solid State Chemistry 2000;149. https://doi.org/10.1006/jssc.1999.8565.

[81] Hyun WJ, Secor EB, Hersam MC, Frisbie CD, Francis LF. High-resolution patterning of graphene by screen printing with a silicon stencil for highly flexible printed electronics. Advanced Materials 2015;27. https://doi.org/10.1002/adma.201404133.

[82] He P, Cao J, Ding H, Liu C, Neilson J, Li Z, et al. Screen-Printing of a Highly Conductive Graphene Ink for Flexible Printed Electronics. ACS Applied Materials and Interfaces 2019;11. https://doi.org/10.1021/acsami.9b04589.

[83] Vicente AT, Araújo A, Mendes MJ, Nunes D, Oliveira MJ, Sanchez-Sobrado O, et al. Multifunctional cellulose-paper for light harvesting and smart sensing applications. Journal of Materials Chemistry C 2018;6:3143–81. https://doi.org/10.1039/c7tc05271e.

[84] WHAT IS SCREEN PRINTING? A STEP-BY-STEP GUIDE n.d. https://www.customplanet.co.uk/what-is-screen-printing-step-by-step-i50 (accessed June 23, 2020).

[85] Mumby R. Printing for packaging. Packaging Technology 2012:441–89. https://doi.org/10.1533/9780857095701.3.441.

[86] Vena A, Perret E, Tedjini S. Implementation and Measurements of Chipless RFID Tags. Chipless RFID based on RF Encoding Particle, 2016. https://doi.org/10.1016/b978-1-78548-107-9.50005-7.

[87] Izdebska J. Flexographic Printing. Elsevier Inc.; 2015. https://doi.org/10.1016/B978-0-323-37468-2.00011-7.

[88] Conheça a INCM n.d. https://www.incm.pt/portal/incm_apresentacao.jsp (accessed June 20, 2020).

[89] Schneider CA, Rasband WS, Eliceiri KW. NIH Image to ImageJ: 25 years of image analysis. Nature Methods 2012;9. https://doi.org/10.1038/nmeth.2089.

[90] Lu F, Zhang J, Huang M, Namavar F, Ewing RC, Lian J. Phase transformation of nanosized ZrO2 upon thermal annealing and intense radiation. Journal of Physical Chemistry C 2011;115. https://doi.org/10.1021/jp109558s.

[91] Kieu Giang LT, Marciniak Ł, Kamil Żur K, Tien DM, Vu N, Binh NT, et al. Zirconium metal organic framework for design of tetragonal rare earth-doped zirconia nanoparticles. Journal of Rare Earths 2019;37. https://doi.org/10.1016/j.jre.2019.03.003.

[92] Miguel T, Silva S. (2018). Upconversion Materials for Security Inks. Faculdade de Ciências e Tecnologias, Lisboa, Portugal).

[93] Souza AE, Santos GTA, Barra BC. TRANSFORMAÇÃO CÍCLICA DA MORFOLOGIA DE CRISTAIS DE TITANATOS ASSOCIADA AO GRAU DE ORDEM-DESORDEM DE CLUSTERS AUTOMONTADOS 2012:2749–60.

[94] Caruso R, de Sanctis O, Macías-García A, Benavidez E, Mintzer SR. Influence of pH value and solvent utilized in the sol-gel synthesis on properties of derived ZrO2 powders. Journal of Materials Processing Technology 2004;152. https://doi.org/10.1016/j.jmatprotec.2004.04.371.

[95] Quintard PE, Barbéris P, Mirgorodsky AP, Merle-Méjean T. Comparative lattice-dynamical study of the Raman spectra of monoclinic and tetragonal phases of zirconia and

hafnia. Journal of the American Ceramic Society, vol. 85, 2002. https://doi.org/10.1111/j.1151-2916.2002.tb00346.x.

[96] Sharma G, Sehgal P, Narula AK. Reviews in Fluorescence 2015. 2015.

[97] Fang Z, Cao R, Zhang F, Ma Z, Dong G, Qiu J. Efficient spectral conversion from visible to near-infrared in transparent glass ceramics containing Ce3+-Yb3+ codoped Y 3Al5O12 nanocrystals. Journal of Materials Chemistry C 2014;2:2204–11. https://doi.org/10.1039/c3tc32231a.

[98] Tian Y, Fu Y, Xing M, Luo X. Upconversion luminescence properties of Y2O3:Yb, Er and Y2O2S:Yb, Er nanoparticles prepared by complex precipitation. Journal of Nanomaterials 2015;2015. https://doi.org/10.1155/2015/573253.

[99] Kassab LRP, Bomfim FA, Martinelli JR, Wetter NU, Neto JJ, de Araújo CB. Energy transfer and frequency upconversion in Yb3+-Er 3+-doped PbO-GeO2 glass containing silver nanoparticles. Applied Physics B: Lasers and Optics 2009;94:239–42. https://doi.org/10.1007/s00340-008-3249-2.

6 Appendixes

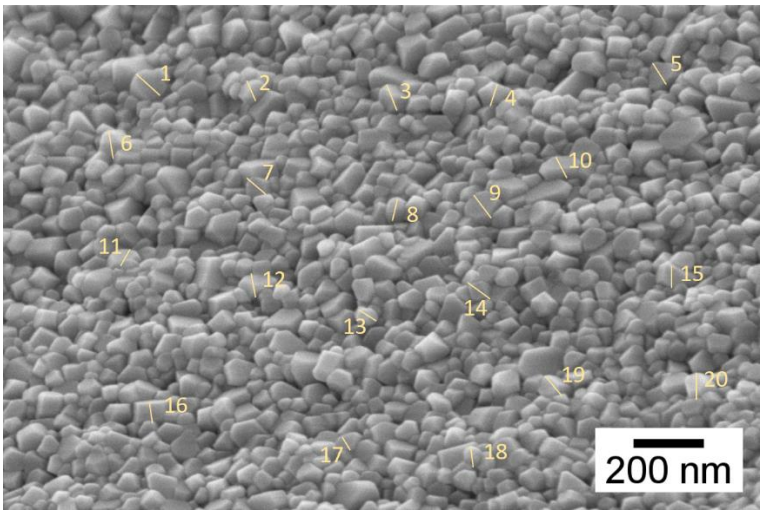

Figure 6.1 – Measures of different nanoparticles from Figure 3.3 (c).

	Label	Area	Mean	Min	Max	Angle	Length
1		152.535	207.971	200.729	212.667	-42.357	82.889
2		103.854	208.350	200.333	212.667	-67.521	56.540
3		133.063	167.236	111.375	203.490	-66.615	72.621
4		116.836	188.923	124.000	212.423	-111.501	63.896
5		136.308	124.196	93.000	138.341	-59.036	73.532
6		146.045	201.872	106.114	212.667	-80.754	78.485
7		126.572	160.193	115.734	211.000	-32.005	67.982
8		136.308	154.304	76.000	201.895	-104.036	74.278
9		142.799	191.193	108.000	212.197	-49.686	77.966
10		133.063	199.749	123.333	212.667	-63.435	72.509
11		123.327	159.732	109.505	184.389	-119.358	66.143
12		123.327	199.955	108.000	212.588	-77.471	66.436
13		110.345	162.971	110.000	201.818	-32.735	59.966
14		136.308	178.596	148.000	212.667	-34.077	73.950
15		113.590	185.071	106.000	212.667	-95.042	61.489
16		103.854	185.569	134.361	211.903	-76.866	55.497
17		94.118	127.984	97.000	149.857	-49.399	49.827
18		116.836	168.852	85.000	227.000	-75.174	63.361
19		172.008	187.299	111.243	214.103	-54.462	92.983
20		162.272	203.014	128.000	212.667	-91.169	88.292
21	Mean	129.168	178.151	119.786	203.484	-69.135	69.932
22	SD	20.023	24.593	32.058	21.899	25.924	11.022
23	Min	94.118	124.196	76.000	138.341	-119.358	49.827
24	Max	172.008	208.350	200.729	227.000	-32.005	92.983

Figure 6.2 – Measures and mean value of Figure 3.3 (c).